AGU PUBLICATIONS

JGR

Journal of Geophysical Research: Solid Earth

RESEARCH ARTICLE
10.1002/2017JB014521

# Earthquake Nucleation on Faults With Heterogeneous Frictional Properties, Normal Stress

**Sohom Ray**[1] **and Robert C. Viesca**[1]

[1]Department of Civil and Environmental Engineering, Tufts University, Medford, MA, USA

**Key Points:**
- Heterogeneous frictional properties and normal stress lead to preferential nucleation sites
- The location of the sites is determined a priori by the property distributions
- Conclusion is drawn from analysis of earthquake nucleation under rate- and state-dependent friction

**Correspondence to:**
S. Ray,
Sohom.Ray@tufts.edu

**Citation:**
Ray, S., & Viesca, R. C. (2017). Earthquake nucleation on faults with heterogeneous frictional properties, normal stress. *Journal of Geophysical Research: Solid Earth*, *122*, 8214–8240. https://doi.org/10.1002/2017JB014521

Received 3 JUN 2017
Accepted 28 SEP 2017
Accepted article online 4 OCT 2017
Published online 28 OCT 2017

**Abstract** We examine the development of an instability of fault slip rate. We consider a slip rate and state dependence of fault frictional strength, in which frictional properties and normal stress are functions of position. We pose the problem for a slip rate distribution that diverges quasi-statically within finite time in a self-similar fashion. Scenarios of property variations are considered and the corresponding self-similar solutions found. We focus on variations of coefficients, $a$ and $b$, respectively, controlling the magnitude of a direct effect on strength due to instantaneous changes in slip rate and of strength evolution due to changes in a state variable. These results readily extend to variations in fault-normal stress, $\sigma$, or the characteristic slip distance for state evolution, $D_c$. We find that heterogeneous properties lead to a finite number of self-similar solutions, located about critical points of the distributions: maxima, minima, and between them. We examine the stability of these solutions and find that only a subset is asymptotically stable, occurring at just one of the critical point types. Such stability implies that during instability development, slip rate and state evolution can be attracted to develop in the manner of the self-similar solution, which is also confirmed by solutions to initial value problems for slip rate and state. A quasi-static slip rate divergence is ultimately limited by inertia, leading to the nucleation of an outward expanding dynamic rupture: asymptotic stability of self-similar solutions then implies preferential sites for earthquake nucleation, which are determined by distribution of frictional properties.

## 1. Introduction

This study considers the quasi-static development of an instability of fault slip as a mechanism for the nucleation of an earthquake-generating dynamic rupture of the fault. This consideration is given within the framework of a slip rate- and state-dependent frictional description. We review observations indicating that frictional strength properties, and, in turn, the parameters underlying their description, likely vary over the extent of fault surfaces. In light of this we examine how an instability develops on faults with such variations, focusing on the nonlinear, late-stage acceleration that is expected to precede the nucleation of a dynamic rupture. We will find that variations in frictional properties lead to preferential nucleation sites that are determined a priori by the properties' distributions.

We consider that a fault's frictional strength is determined by both the instantaneous rate of slip and the slip rate history, or state. Specifically, we consider the description formulated by Ruina (1983) on the basis of rock friction experiments conducted at low sliding rates representative of the interseismic period (e.g., Dieterich, 1978, 1979; Ruina, 1983). Salient features of the observed rate and state dependence include a so-called direct effect, in which changes in sliding rate are instantaneously matched with changes of the same sign in frictional strength. Additionally, following a change to a fixed sliding rate, the frictional strength is observed to evolve to a steady value over a characteristic amount of slip. Moreover, this apparent steady state value of frictional strength is observed to be either an increasing or decreasing function of the slip rate. There are several lines of evidence indicating these observed properties vary in magnitude over a given fault.

The foremost indication follows from the early determination that some of the above properties clearly depend on the ambient temperature. A large number of studies have examined or permitted the inference of the temperature dependence of the direct effect magnitude on both an experimental and theoretical basis (Baumberger et al., 1999; Blanpied et al., 1991, 1995, 1998; Brechet & Estrin, 1994; He et al., 2007; Heslot et al., 1994; Nakatani, 2001; Persson, 2000; Rice et al., 2001; Stesky, 1975, 1978; Stesky et al., 1974). A robust observation is an apparently linear dependence of the magnitude of the direct effect on temperature, generally thought to follow from the assumption that the slip rate is in part determined by a thermally activated process.

Seismological and geodetic observations have also been used to infer variations of frictional properties. Geodetic inferences include inversion for the magnitude of the direct and evolution effects or steady state rate dependence, which indicate variations of each at the crustal scale (Jolivet et al., 2013; Kaneko et al., 2013; Lindsey & Fialko, 2016), and also include patterns of interseismic coupling suggesting transitions between rate-strengthening and rate-weakening behavior, again on the crustal scale (e.g., Chlieh et al., 2008; Jolivet et al., 2015; Kaneko et al., 2010; Perfettini et al., 2010; Villegas-lanza et al., 2016). Finer-scale variations are suggested by seismological observations, which include precise relocations of microseismicity (e.g., Rubin et al., 1999; Waldhauser et al., 2004) that show clustering interspersed by comparatively quiescent regions. These last observations suggest a potentially mottled fault frictional behavior in which regions capable of the spontaneous emergence of microseismicity are embedded within an otherwise stably creeping fault. This image is further supported, for example, when considering relations between seismic moment and interevent time of repeating seismicity (Nadeau & Johnson, 1998) that are well explained by models that appeal to rate-weakening patches embedded within an otherwise rate-strengthening fault (Chen & Lapusta, 2009).

Field and laboratory studies identify a multitude of on-fault and external conditions that may be responsible for spatial variations of frictional properties. Samples from exhumed and drilled faults show varied fault gouge composition or fabric, which has been identified as contributing to strength variations (e.g., Carpenter et al., 2014; Collettini et al., 2009; Ikari et al., 2014; Niemeijer & Vissers, 2014; Tesei et al., 2014; Wojatschke et al., 2016). Such compositional variation may be due to the variability of the fault wall rock type or due to alteration of fault gouge composition or structure. For instance, laboratory measurements show that the characteristic slip distance for strength evolution is correlated with fault gouge thickness (e.g., Marone, 1998; Marone & Kilgore, 1993). Additionally, migration of aqueous fluid facilitates spatially variable chemical alterations of the minerals (e.g., Evans & Chester, 1995; Stierman, 1984; Wintsch et al., 1995).

Temperature dependence of frictional properties alone has motivated early seismic cycle models coupling rate- and state-dependent friction to the deformation of elastic continua in contact (e.g., Lapusta et al., 2000; Rice, 1993; Tse & Rice, 1986). Here the observed dependence is used as evidence for a transition in behavior with depth from potentially unstable rate weakening, which permits the nucleation and propagation of an earthquake rupture, to stable rate strengthening, which results in steady creep at depth. Apart from a narrow transition zone, frictional properties are typically assumed to be uniform throughout the rate-weakening interval, largely to maintain model simplicity. However, several studies have begun to examine how heterogeneous distributions of frictional properties affect the earthquake cycle (e.g., Barbot et al., 2012; Hillers et al., 2006), including correlations between final earthquake size and property distributions (Hillers et al., 2007).

Prior analyses of the stability of interfaces of elastic continua following rate- and state-dependent frictional strength has been limited to interfaces with uniform frictional properties and normal stress. Rice and Ruina (1983) and Rice et al. (2001) examined the linear stability of uniform steady state sliding and found that such sliding was stable to perturbations provided the perturbation wavelength was below a critical value. This critical wavelength was independent of the particular form of so-called state evolution laws, provided their linearizations coincide. Subsequent work investigated the progression of instability into the nonlinear regime, in which the particular form of the state evolution law becomes important. Dieterich (1992) and Rubin and Ampuero (2005) examined instability development under the so-called aging-law form of the state evolution and found characteristic length over which slip rate accelerated which differs from the critical wavelength identified previously. In contrast, when examining the instability development under an alternative state evolution law, the so-called slip law, Ampuero and Rubin (2008) and Rubin and Ampuero (2009) found that the slip rate appears to accelerate unstably with a vanishing length scale.

While the nonlinear aspect of later stages of instability development shifts focus of investigations toward numerical solutions, analytical insight was gained, in particular, when Rubin and Ampuero (2005) found the existence of a self-similar solution for instability development, under aging-law state evolution. Specifically, the solution involved a finite-time divergence of slip rate with a fixed spatial distribution and was found to exist over a given range of a sole problem parameter (the ratio of coefficients moderating the direct and evolution effects). Furthermore, numerical solutions for slip rate evolution within this parameter range that tracked the progression of the slip rate instability were observed to asymptotically converge to the self-similar solution; however, no such behavior was directly observed in their work outside of this parameter range and instead slip rate acceleration appeared to give way to complex, unpredictable spatiotemporal patterns.

Viesca, (2016a, 2016b) subsequently examined nonlinear instability development under the aging-law state evolution and found several additional analytical results. First, self-similar solutions exist over the entire range

of the problem parameter (the ratio of direct and evolution effect coefficients). Second, these self-similar solutions could be understood as fixed points of a dynamical system, which provides a framework to determine whether the solutions are attractive and attainable. Third, the solutions were found to be unconditionally attractive for the parameter range identified by Rubin and Ampuero (2005) but were found to be unstable outside of this range, and chaotically so within a particular range.

Here we look to further develop the results of Viesca, (2016a, 2016b) to consider the role of heterogeneities in frictional properties and normal stress in the development of earthquake-nucleating slip instabilities. In section 2, we discuss fault frictional strength and stress, which provides governing equations. In section 3, we consider the evolution of strength and stress during an instability and look for self-similar solutions for an unstably accelerating slip rate under general variations in frictional properties and normal stress. In section 4, we highlight two parameters of particular interest (the direct and evolution effect coefficients) as well as two characteristic models of elastic continua with embedded slip surfaces relevant for models of fault, landslide, or ice stream slip instabilities. In section 5, we find self-similar solutions for these specific sets of parameters and models and assess their stability in section 6. To demonstrate the validity of our results, we compare our analysis with numerical solutions to the evolution equations for slip rate and state in section 7.

## 2. Fault Stress and Frictional Strength

A geological fault is represented here as an interface, within a continuum, across which relative displacement may occur. Here we presume that the displacement of one side of the interface with respect to the opposing side is a vector of uniform direction, tangent to the interface, but of a variable magnitude, denoted by $\delta(\boldsymbol{x}, t)$ where $\boldsymbol{x}$ is a vector whose components indicate a position on the fault surface, and $t$ is time. The relative displacement magnitude $\delta$ is identified as the fault slip increment with respect to slip accumulated up to $t = 0$. We denote $\tau$ as the magnitude of the shear traction on the fault plane and assume that it may be decomposed into two principal components:

$$\tau(\boldsymbol{x}, t) = \tau_{\text{el}}(\boldsymbol{x}, t) + \tau_{\text{ex}}(\boldsymbol{x}, t) \tag{1}$$

We define $\tau_{\text{ex}}(\boldsymbol{x}, t)$ as the magnitude of the shear tractions that would exist on the fault interface if the fault remains locked at its reference state (i.e., $\delta$ maintained uniformly 0). $\tau_{\text{ex}}(\boldsymbol{x}, t)$ can then be identified as having two possible sources: that is, a contribution due to a history of slip preceding the reference point in time, which may be spatially heterogeneous, but remains constant forward in time; and a potentially time-dependent contribution arising from sources of external forcing, which lead to the accumulation of shear traction on the interface under a locked fault.

The remaining component, $\tau_{\text{el}}$, corresponds to shear traction change due slip $\delta$. Specifically, under quasi-static elastic deformation of the fault-bounding medium, $\tau_{\text{el}}$, at any position $\boldsymbol{x}$ on the fault, depends on the instantaneous slip distribution $\delta(\boldsymbol{x}, t)$ on the fault (e.g., Bilby & Eshelby, 1968; Rice, 1968). We represent this relation by an operator $\mathcal{L}$, which operates on a slip distribution and gives stress at any desired position as given below:

$$\tau_{\text{el}}(\boldsymbol{x}, t) = \mathcal{L}[\delta(\boldsymbol{x}, t); \boldsymbol{x}] \tag{2}$$

The operator $\mathcal{L}$ is a boundary representation of a stress-displacement relation from elastic dislocation theory of which the underlying governing equations (stress-strain and strain-displacement relations, and equilibrium equations) are all linear. As a result, $\mathcal{L}$ is a linear operator acting only on the instantaneous spatial distribution of $\delta$. In other words, $\mathcal{L}$ has properties such that

$$\mathcal{L}[\alpha(t)g(\boldsymbol{x}) + \beta(t)h(\boldsymbol{x}); \boldsymbol{x}] = \alpha(t)\mathcal{L}[g(\boldsymbol{x}); \boldsymbol{x}] + \beta(t)\mathcal{L}[h(\boldsymbol{x}); \boldsymbol{x}] \tag{3}$$

Additionally, $\mathcal{L}$ has the property that

$$\mathcal{L}\left[\frac{\partial}{\partial t}\delta(\boldsymbol{x}, t); \boldsymbol{x}\right] = \frac{\partial}{\partial t}\mathcal{L}\left[\delta(\boldsymbol{x}, t); \boldsymbol{x}\right]$$

such that we may write

$$\frac{\partial \tau_{\text{el}}}{\partial t} = \mathcal{L}[v(\boldsymbol{x}, t); \boldsymbol{x}] \tag{4}$$

where $v = \partial\delta/\partial t$ is the slip rate.

We assume that the strength of the fault is purely frictional, given by

$$\tau_s(\boldsymbol{x}, t) = \sigma(\boldsymbol{x}, t) f(\boldsymbol{x}, t) \tag{5}$$

where $\sigma$ is the fault-normal stress and $f$ is the friction coefficient. In the case of a fluid-saturated fault zone, $\sigma$ is the effective fault-normal stress, given by $\sigma(\boldsymbol{x}, t) = \sigma_n(\boldsymbol{x}, t) - p(\boldsymbol{x}, t)$, where $\sigma_n$ is the total normal stress and $p$ is the pore fluid pressure on the fault surface.

We consider a rate- and state-dependent constitutive formulation of frictional strength (e.g., Dieterich, 1978; Ruina, 1983). In this framework, the coefficient of friction $f$ at a position on the fault is a function of the instantaneous slip rate $v$, a state variable $\theta$, and material parameters $a$ and $b$ at that position and is expressed as

$$f(\boldsymbol{x}, t) = f_o + a(\boldsymbol{x}) \ln \left[ \frac{v(\boldsymbol{x}, t)}{v_o} \right] + b(\boldsymbol{x}) \ln \left[ \frac{\theta(\boldsymbol{x}, t)}{\theta_o} \right] \tag{6}$$

The state variable $\theta$ contains information on the history of sliding. Here we consider aging-law state evolution (Dieterich, 1979), represented as

$$\frac{\partial \theta}{\partial t} = 1 - \frac{v(\boldsymbol{x}, t)\theta(\boldsymbol{x}, t)}{D_c(\boldsymbol{x})} \tag{7}$$

When the contact surfaces are stationary, then $\theta$ grows proportionally to the contact time or age. Here $D_c$ is the characteristic slip distance over which friction evolves. In steady state, $\partial\theta/\partial t = 0$ and the steady state friction coefficient is

$$f_{ss}(\boldsymbol{x}, t) = f_o + [a(\boldsymbol{x}) - b(\boldsymbol{x})] \ln \left[ \frac{v(\boldsymbol{x}, t)}{v_o} \right] \tag{8}$$

In (6) and above, $f_o$ is the reference coefficient of friction at steady state sliding velocity $v_o$ and state $\theta_o = D_c/v_o$. The parameters $a$ and $b$ are the properties of the contacting surfaces and are inferred from laboratory experiments to be of the order of $10^{-2}$. The parameter $a$ moderates the magnitude of the immediate change of friction in response to a sudden jump in steady state sliding velocity and is denoted as the direct effect coefficient. The parameter $b$ moderates the magnitude of the effect of the state variable and state evolution and is referred to as an evolution effect coefficient. For a sudden jump in velocity, the evolution effect results in friction evolving to a new steady state over the characteristic slip scale $D_c$. When $a < b$, the surface is steady state rate weakening. Here we have allowed for $a$, $b$, and $D_c$ to be functions of position on the fault.

To close the model, a frictional strength description requires that the total shear traction equals the frictional strength, that is,

$$\tau(\boldsymbol{x}, t) = \tau_s(\boldsymbol{x}, t)$$

when and where the fault is sliding.

As mentioned previously, the above system is known to be linearly unstable to perturbations about a steady state if the frictional interface is steady state rate-weakening ($a - b < 0$). Specifically, the instability is manifested as a divergence in sliding rate with time. In the next section, we begin by stating how that divergence progresses in the nonlinear regime (i.e., beyond the linear regime of the prior stability analysis) and then consider what are the implications for the evolution of shear stress and shear strength during this rapid acceleration phase. In light of these considerations, we will search for solutions for quasi-statically diverging slip rate, allowing for spatial heterogeneity in frictional parameters and effective normal stress.

## 3. Analysis of the Nonlinear Instability of Sliding Rate on Heterogeneous Interfaces

On the basis of scaling considerations of the resulting evolution equations we may deduce that during a sliding instability, slip rate evolution follows the scaling $\partial v/\partial t \sim v^2/D_c$ (e.g., Viesca, 2016a), which implies slip rate diverging as

$$v(x, t) \sim D_c/t_f(t) \tag{9}$$

where $t_f(t) = t_{\text{in}} - t$ denotes the time away from an instability time $t_{\text{in}}$. Alternatively, we may have posited the existence of a finite-time divergence in slip rate, in which no memory of initial conditions or external forcing are retained. This leaves the above scaling as the only means of construction a slip rate dimensionally when considering elastic deformation and frictional response alone (e.g., as also noted by Noda et al., 2013). In the

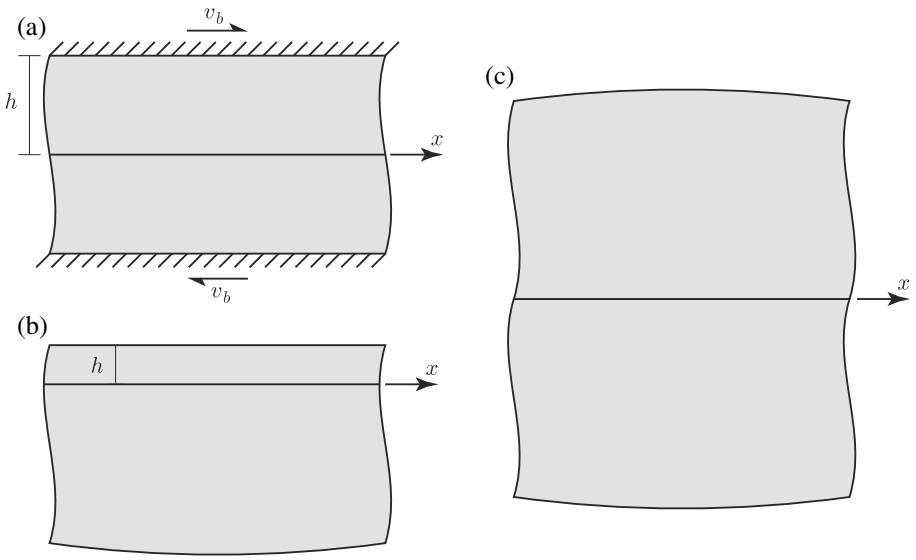


**Figure 1.** Schematic illustration of several model fault scenarios of a planar slip surface, along which lies one direction $x$, embedded within an elastic continuum. (a) This example illustrates a particular choice of model forcing condition: a layer of finite thickness $2h$ undergoes a prescribed displacement rate of magnitude $v_b$ at the top and bottom boundaries. (b and c) Two end-member scenarios of interactions among the points on the surface mediated by the elastic response of the adjoining continua. In Figure 1b the fault surface is located parallel to and a depth $h$ below a free surface at the top; we consider conditions in which variations along the fault occur over distances much larger than $h$, which results in short-ranged (local) interactions between the points on the slip surface. In contrast, for sliding at the interface of two contacting elastic half-spaces (Figure 1c), there is a long-range (nonlocal) interaction between points along the surface.

following we first consider the implications for strength and stress evolution when slip rate diverges in the manner of (9) and then proceed to search for self-similar solutions to the nonlinear problem.

### 3.1. Rate of Shear Stress and Strength Evolution During Instability

We now consider the effect of this divergence on the rate form of our frictional strength criterion

$$\frac{\partial \tau}{\partial t} = \frac{\partial \tau_s}{\partial t} \tag{10}$$

On one hand, the rate of shear stress is simply

$$\frac{\partial \tau}{\partial t} = \frac{\partial \tau_{\text{el}}}{\partial t} + \frac{\partial \tau_{\text{ex}}}{\partial t} \tag{11}$$

where the first term depends on the sliding rate as in (4) and, consequently, also diverges as $1/t_f$ as instability is approached. The specifics of the second term depends on the particulars of the fault location and external sources of stress, but it may be generally expected that the stressing of the fault by external forces follows a bounded rate, implying that the second term will eventually be negligible in comparison with the first. Consider, for instance, the model geometry of Figure 1a. Here

$$\frac{\partial \tau_{\text{ex}}}{\partial t} = \frac{\mu}{h} v_b$$

which is not only bounded but constant in time and uniform in space. Therefore, $\partial \tau_{\text{el}}/\partial t$, the expression for which may be deduced from the solution for an edge dislocation in a strip (e.g., as given implicitly by Horowitz & Ruina, 1989), will quickly come to be the dominant contributor to shear stress rate as the instability is approached.

On the other hand, the rate of shear strength is

$$\frac{\partial \tau_s}{\partial t} = \frac{\partial \sigma}{\partial t} f + \sigma \frac{\partial f}{\partial t} \tag{12}$$

When slip rate diverges as (9), the friction coefficient $f$ and its rate $\partial f/\partial t$ scale as $\log(t_f)$ and $1/t_f$, respectively. When the rate of the effective normal stress rate is bounded, $f\partial\sigma/\partial t$ can be neglected in comparison with

$\sigma \partial f / \partial t$. This is the case, for instance, when the evolution of effective normal stress is due solely to sources not coupled with slip or slip rate, such as changes in pore pressure due to a fluid source or fluid migration.

However, there are scenarios where the terms in (12) may be comparable during a developing instability: specifically, when the evolution of the effective normal stress is itself linked to slip or slip rate. This may be the case, for instance, when considering the dilatancy or compaction of a fluid-saturated fault gouge. Under conditions of rapid deformation, such that evolution of porosity occurs on shorter time scales than fluid migration (undrained conditions), the rate of fluid pressure (and, consequently, effective normal stress) is proportional to the rate of porosity. Simple models for dilatancy may link that rate of porosity directly to slip rate by way of an angle of dilatancy, such that if slip rate diverges, the rate of porosity, and hence, effective normal stress does so similarly. More realistic porosity evolution models (e.g., Segall & Rice, 1995), based on lab experiments monitoring porosity evolution in sheared gouges (e.g., Marone et al., 1990), imply a weaker dependence of porosity on sliding rate but may nonetheless lead to a comparable divergence of the effective normal stress rate for a slip rate diverging as (9). Likewise, fluid pressure may also evolve due to rapid shear heating of saturated fault gouge under an accelerating slip rate, in a process known as thermal pressurization (e.g., Lachenbruch, 1980; Mase & Smith, 1987). For example, under undrained, adiabatic conditions, the rate of effective normal stress is proportional to the sliding rate. Another mechanism to alter effective normal stress is via alterations to the total normal stress, which may occur, for example, when slip occurs along or near a bimaterial interface or other boundary (e.g., Head, 1953). In these cases, the rate of total normal stress changes may be written as an operation analogous to (4), such that the total normal stress rate diverges similarly with slip rate although, in some instances, these normal stress variations may be negligible (see, e.g., supporting information in Viesca, 2016b).

Prior work has examined the interplay of such slip-dependent mechanisms with the frictional description in the development of interfacial sliding instabilities (e.g., Schmitt et al., 2011; Segall et al., 2010); however, here we restrict ourselves to examining the case in which the rate of effective normal stress rate remains bounded to simplify analysis. In this case, the appropriate asymptotic analysis of instability development is to treat the normal stress coefficient in (12) as frozen at its value at time $t = t_{\text{in}}$, and we update the notation to reflect this, that is,

$$\sigma(\boldsymbol{x}, t_{\text{in}}) \Rightarrow \sigma(\boldsymbol{x})$$

As a result, under the conditions of diverging slip rate examined above, the frictional strength condition in rate form is reduced to

$$\frac{\partial \tau_{\text{el}}}{\partial t} = \sigma(\boldsymbol{x}) \frac{\partial f}{\partial t} \tag{13}$$

### 3.2. Search for Solutions of Diverging Slip Rate Under Heterogeneous Frictional Properties and Normal Stress

We begin with the ansatz that slip rate diverges as

$$v(\boldsymbol{x}, t) = \frac{D_c(\boldsymbol{x})}{t_f(t)} \mathcal{W}(\boldsymbol{x}) \tag{14}$$

where $\mathcal{W}(\boldsymbol{x})$ is a to-be-determined positive distribution. The evolution of the state variable follows by substituting the ansatz in the aging law

$$\frac{\partial \theta}{\partial t} = 1 - \frac{\mathcal{W}(\boldsymbol{x})}{t_f(t)} \theta(\boldsymbol{x}, t) \tag{15}$$

which has the solution, to within a temporal constant of integration $C(\boldsymbol{x})$,

$$\theta(\boldsymbol{x}, t) = C(\boldsymbol{x}) [t_f(t)]^{\mathcal{W}(\boldsymbol{x})} + \frac{t_f(t)}{\mathcal{W}(\boldsymbol{x}) - 1} \tag{16}$$

In the limit $t_f \to 0$, the leading order term of $\theta(\boldsymbol{x}, t)$ is either given by the first or the second term if $\mathcal{W} \leq 1$ or $\mathcal{W} > 1$, respectively, implying the state variable $\theta(\boldsymbol{x}, t)$ evolves as

$$\frac{1}{\theta(\boldsymbol{x}, t)} \frac{\partial \theta}{\partial t} = -\frac{1}{t_f(t)} \begin{cases} \mathcal{W}(\boldsymbol{x}) & \mathcal{W}(\boldsymbol{x}) \leq 1 \\ 1 & \mathcal{W}(\boldsymbol{x}) > 1 \end{cases} \tag{17}$$

Consequently, considering that from (6),

$$\frac{\partial f}{\partial t} = \frac{a(\boldsymbol{x})}{v(\boldsymbol{x},t)}\frac{\partial v}{\partial t} + \frac{b(\boldsymbol{x})}{\theta(\boldsymbol{x},t)}\frac{\partial \theta}{\partial t} \tag{18}$$

we can express the rate of the friction coefficient as

$$\frac{\partial f}{\partial t} = \frac{1}{t_f(t)}\begin{cases} a(\boldsymbol{x}) - b(\boldsymbol{x})\mathcal{W}(\boldsymbol{x}) & \mathcal{W}(\boldsymbol{x}) \le 1 \\ a(\boldsymbol{x}) - b(\boldsymbol{x}) & \mathcal{W}(\boldsymbol{x}) > 1 \end{cases} \tag{19}$$

This, along with the stress-strength balance (13), casts the problem to determine the as-of-yet unknown distribution $\mathcal{W}(\boldsymbol{x})$, as finding the distribution that satisfies

$$\mathcal{L}[D_c(\boldsymbol{x})\mathcal{W}(\boldsymbol{x});\boldsymbol{x}] = \sigma(\boldsymbol{x})\begin{cases} a(\boldsymbol{x}) - b(\boldsymbol{x})\mathcal{W}(\boldsymbol{x}) & \mathcal{W}(\boldsymbol{x}) \le 1 \\ a(\boldsymbol{x}) - b(\boldsymbol{x}) & \mathcal{W}(\boldsymbol{x}) > 1 \end{cases} \tag{20}$$

This problem is mathematically equivalent to that determining the slip distribution of a shear crack, with a piecewise linearly slip-weakening friction, that is, in equilibrium with a background shear stress distribution, given below

$$\tau_b(\boldsymbol{x}) + \mathcal{L}[\delta(\boldsymbol{x},t);\boldsymbol{x}] = \sigma(\boldsymbol{x})\begin{cases} f_p(\boldsymbol{x}) - [f_p(\boldsymbol{x}) - f_r(\boldsymbol{x})]\dfrac{\delta(\boldsymbol{x})}{\delta_c(\boldsymbol{x})} & \dfrac{\delta(\boldsymbol{x})}{\delta_c(\boldsymbol{x})} \le 1 \\ f_r(\boldsymbol{x}) & \dfrac{\delta(\boldsymbol{x})}{\delta_c(\boldsymbol{x})} > 1 \end{cases} \tag{21}$$

where $f_p$ and $f_r$ are the peak and residual friction coefficients, $\delta_c$ is the critical slip distance beyond which $f = f_r$, and $\sigma$ and $\tau_b$ are fault-normal and background (i.e., initial) shear stresses. We compare (20) and (21), to find the following equivalences

$$\begin{aligned} a(\boldsymbol{x}) &\Leftrightarrow f_p(\boldsymbol{x}) - \tau_b(\boldsymbol{x})/\sigma(\boldsymbol{x}) \\ b(\boldsymbol{x}) &\Leftrightarrow f_p(\boldsymbol{x}) - f_r(\boldsymbol{x}) \\ D_c(\boldsymbol{x}) &\Leftrightarrow \delta_c(\boldsymbol{x}) \\ \mathcal{W}(\boldsymbol{x}) &\Leftrightarrow \delta(\boldsymbol{x})/\delta_c(\boldsymbol{x}) \end{aligned}$$

The problem of determining $\mathcal{W}(\boldsymbol{x})$ is one of also determining its domain: that is, the problem for $\mathcal{W}$ involves a stationary free boundary. We denote $\boldsymbol{x} = \boldsymbol{x_b}$ as the position of the boundary of compact support for $\mathcal{W}$. In the slip-weakening crack context, the necessary additional constraint comes from the requirement of the absence of a crack tip stress singularity (i.e., the stress at the crack tip is the peak strength given by $\sigma(\boldsymbol{x_b})f_p(\boldsymbol{x_b})$). Given the Williams expansion for crack tip stress fields (Williams, 1957), eliminating the stress singularity ahead of the crack edge amounts to requiring that the boundary-normal gradient of slip $\delta$ vanish as the boundary is approached. The equivalent condition on $\mathcal{W}$ implies that the singularity in stress rate arrives only through the $1/t_f$ divergence of slip rate. In both contexts this condition is applied assuming that there are no circumstances that lock or pin a region of the slip surface against sliding, such that a singularity in stress or stress rate may occur.

In the next section, we discuss classes of frictional parameter and normal stress heterogeneity and elastic fault configurations. After, in section 5, we find solutions for the distribution $\mathcal{W}$ for specific variations in each class. Therein, we find that heterogeneous distributions determine a finite number of potential nucleation sites. In section 6, we determine that among these potential sites, only a subset may be preferred nucleation sites. This is determined by a linear stability analysis of the slip rate blowup solutions. In section 7, we compare the results of the above analysis to numerical solutions of the slip rate and state evolution equations.

## 4. Frictional Property Distributions and Model Fault Geometry

In the preceding section we posed the problem of a quasi-static slip rate instability as one with a known rate of divergence and a to-be-determined spatial distribution $\mathcal{W}$ under conditions of generic spatial variation of normal stress $\sigma$ and frictional parameters $a$, $b$, and $D_c$. Proceeding toward solutions for that distribution, we first classify types of variations in parameters as well as end-members of a range of potential embedded fault geometries. We will find that when considering the problem for the distribution $\mathcal{W}$, some parameter variation types may be equivalent to one another, which reduces the number of cases that need to be studied. Additionally, we will classify interactions of points on the slip surface (mediated by the elasticity of the contacting bodies) according to the spatial range over which they occur, which will depend on the geometry of the medium hosting the fault.

### 4.1. Categorizing Frictional Parameter Heterogeneity

We are interested in how a variation in any of the frictional parameters may affect the development of slip instability, how variations in more than one parameter may compete, and whether any parameter exerts a preeminent control on earthquake nucleation.

To begin, we will consider the variations of the direct and evolution effect coefficients $a$ and $b$ under uniform $\sigma$ and $D_c$. One option is to explicitly vary each; however, given their role in determining the character of steady state rate-weakening behavior, we choose to consider variations posed otherwise. Specifically, we prescribe variations of the absolute *magnitude* of (steady state) logarithmic rate-weakening

$$m(\boldsymbol{x}) = b(\boldsymbol{x}) - a(\boldsymbol{x})$$

as well as variations in *relative* magnitude of (steady state) rate-weakening coefficient

$$r(\boldsymbol{x}) = \frac{b(\boldsymbol{x}) - a(\boldsymbol{x})}{b(\boldsymbol{x})}$$

where the choice to scale $m$ by $b$ (and not $a$) is arbitrary and inconsequential. In choosing variations of $m$ and $r$ we are implicitly varying $a$ and $b$ as $b(\boldsymbol{x}) = m(\boldsymbol{x})/r(\boldsymbol{x})$ and $a(\boldsymbol{x}) = m(\boldsymbol{x})(1-r(\boldsymbol{x}))/r(\boldsymbol{x})$. In this form, the strongest absolute and relative rate weakening correspond to the maximum of $m(\boldsymbol{x})$ and $r(\boldsymbol{x})$, respectively.

A first case to consider is variations of *absolute* and *relative* magnitudes of rate weakening that occur in concert. Such a variation may be achieved by prescribing a spatial variation of either $a$ or $b$ and keeping the other constant. In this case, given that the maximums and minimums coincide, one might readily presume that there would be a preference for slip instability to occur about local maxima, where steady state rate weakening is strongest in both senses. That such a variation may lead to a preferential location for the distribution of $\mathcal{W}$ may also be anticipated by considering the equivalent slip-weakening crack problem. We recall that problem corresponds to determining and locating the distribution of slip for a shear crack with slip-weakening friction in equilibrium with background shear stress. A variation of $a$ under a uniform value of $b$ (in addition to uniform $\sigma$ and $D_c$) is analogous to a variation of the background shear stress $\tau_b$ (under uniform $\sigma$, $f_p$, $f_r$, and $\delta_c$): the resulting maximum in rate weakening ($m$ or $r$) corresponds, respectively, to a maximum in $\tau_b$, which determines a preferential location for a shear crack.

In contrast, we will also examine variations in which the absolute and relative magnitude of relative rate weakening are varied out of concert, that is, such that a maximum of $m(\boldsymbol{x})$ is a minimum of $r(\boldsymbol{x})$, or the converse. Such a case will serve to determine whether the absolute or relative magnitude is the determining factor for the development of a slip instability (all other parameters held uniform). Additionally, we will also examine variations of either the absolute or relative rate weakening while the other is held uniform. This will permit a determination of the influence each alone has on instability development.

Specific variations of $r$ and $m$ have an equivalence to variations of fault-normal stress $\sigma$ and slip evolution distance $D_c$. A spatial variation of the effective normal stress $\sigma$ (with $a$, $b$, and $D_c$ held uniform) is equivalent to that of a spatial variation in $m$ under uniform $r$ (with and $D_c$ and $\sigma$ also held uniform). This is apparent because $\sigma$ enters as a product with $b$ and $a$ such that the difference of $\sigma(\boldsymbol{x})a$ and $\sigma(\boldsymbol{x})b$ is a function of position whereas the ratio of those two quantities is not. Thus, by prescribing a function $m(\boldsymbol{x})$ and holding $r$ to be uniform, we implicitly consider the effect of nonuniform $\sigma$. Similar considering the problem of determining $\mathcal{W}$ (20), we find that nucleation under spatially variable $D_c$ can in some cases be considered in terms of an equivalent problem in which $b$ varies in space and $a$, $\sigma$, and $D_c$ are uniform. We recall that this latter problem corresponds to $r$ and $m$ varying in concert.

### 4.2. Settings of Slip Surfaces in Elastic Bodies and the Extent of Elastic Interactions

The friction coefficient at a point on a sliding surface is determined by the slip rate and its history at that point; points in space are coupled by elasticity of the contacting media such that slip at one point induces a change in shear tractions at another point on the surface. We choose to examine two fault models that span the potential range of interaction between points on the slip surface from long to short. In both models, the variations of quantities on the slip surface (both problem parameters and variables) are assumed to occur along one dimension, $x$.

The first end-member model is one in which elastic interactions are short ranged. Specifically, we consider a slip surface, within a half-space, that is parallel to the free surface and at a depth $h$ below, and furthermore,

**Table 1**
*Variables and Nondimensional Parameters*

| Variable parameter | Length scale (thin-slab) | Length scale (half-spaces) |
|---|---|---|
| $b(x)$, $a(x)$ | $L_{\mathrm{nh}} = \sqrt{\bar{E}hD_c/\sigma}$ | $L_n = \bar{\mu}D_c/\sigma$ |
| $a(x)$ only | $L_{\mathrm{bh}} = \sqrt{\bar{E}hD_c/\sigma b}$ | $L_b = \bar{\mu}D_c/\sigma b$ |

*Note.* $\bar{E} = 2\mu/(1-\nu)$ (mode II) or $\mu$ (mode III); $\bar{\mu} = \mu/(1-\nu)$ (mode II) or $\mu$ (mode III).

under the condition that variations along the slip surface are much greater than the depth $h$. In this limit, the behavior is one of a layer, whose deformation is uniform in depth, overriding an effectively rigid substrate, despite having uniform elastic moduli (see, e.g., supporting information in Viesca, 2016b): that is, slip along the interface is wholly accommodated by deformation of the overriding layer, which only varies in $x$. That deformation may either be in-plane or out-of-plane, such that slip is either mode II or mode III, respectively. This fault model is referred to here as a thin-slab or thin-layer model. The elastic interaction of the points on the slip surface is local in nature and the operator $\mathcal{L}$ acting on the distribution of slip $\delta(x,t)$ is (supporting information Viesca, 2016b)

$$\mathcal{L}[\delta(x,t);x] = \bar{E}h\frac{\partial^2\delta(x,t)}{\partial x^2} \tag{22}$$

where the elastic modulus $\bar{E} = 2\mu/(1-\nu)$ and $\bar{E} = \mu$ for mode-II and mode-III sliding, respectively. $\mu$ and $\nu$ are the shear modulus and Poisson's ratio, respectively.

The second end-member model is one in which elastic interactions are long ranged. Such interactions occur for slip at the interface between two elastic half-spaces. The operator $\mathcal{L}$ operating on a distribution of slip varying along $x$ is given by

$$\mathcal{L}[\delta(x,t);x] = \frac{\bar{\mu}}{2\pi}\int_{-\infty}^{\infty}\frac{\partial\delta(\xi,t)/\partial\xi}{\xi - x}\mathrm{d}\xi \tag{23}$$

where $\bar{\mu} = \mu/(1-\nu)$ and $\bar{\mu} = \mu$ for in-plane and antiplane slip, respectively. The integrand is singular at $\xi = x$, and the integral is evaluated in a Cauchy principal value sense. The nonlocal (long-range) character of the interaction between points on the fault is evident in that $\mathcal{L}$ takes the form of a convolution operation.

Thus, given a particular fault model and choice of parameter variations, we may solve for the slip rate distribution $\mathcal{W}$ of (14). We look for distributions $\mathcal{W}$ with compact support, that is, with a domain on $x$ within an interval $[L_-, L_+]$. Given the highlighted equivalence of the problem, (20), posed for $\mathcal{W}$ with variable $D_c$ or $\sigma$ (and fixed $a$, $b$) to the problem posed with variable $a$ or $b$ (and uniform $\sigma$, $D_c$), we focus on the case assuming uniform $D_c$ and $\sigma$ are constant and will return to consider their variation in light of the results to follow.

For uniform $\sigma$ and $D_c$, the spatial distribution $\mathcal{W}$ for the thin layer scenario must satisfy

$$\frac{\bar{E}hD_c}{\sigma}\frac{\mathrm{d}^2\mathcal{W}}{\mathrm{d}x^2} = \begin{cases} a(x) - b(x)\mathcal{W}(x) & \mathcal{W}(x) \le 1 \\ a(x) - b(x) & \mathcal{W}(x) > 1 \end{cases} \tag{24a}$$

and at the interface between two half-spaces is given by

$$\frac{\bar{\mu}D_c}{2\pi\sigma}\int_{L_-}^{L_+}\frac{\mathrm{d}\mathcal{W}/\mathrm{d}\xi}{\xi - x}\mathrm{d}\xi = \begin{cases} a(x) - b(x)\mathcal{W}(x) & \mathcal{W}(x) \le 1 \\ a(x) - b(x) & \mathcal{W}(x) > 1 \end{cases} \tag{24b}$$

In both the cases, we are to solve for the interval $\Omega$ and the distribution $\mathcal{W}(x)$ therein. The required boundary conditions are $\mathcal{W} = 0$ and $\mathrm{d}\mathcal{W}/\mathrm{d}x = 0$ at $x = L_-$ and $x = L_+$. The former boundary condition ensures continuity of slip rate on $x$, and the latter boundary condition, as discussed in section 3.2, ensures there is no singular shear stress rate, apart from that owed to the $1/t_f$ divergence of slip rate. We denote the half-width of the nucleating patch as $L = (L_+ - L_-)/2$. This width and other, along-fault distances, may be measured with respect to natural elastofrictional length scales that may be deduced from the dimensional prefactors on the left-hand side of (24a,b); the resultant length scales are proportional to $\sqrt{\mu D_c h/\sigma}$ and $\mu D_c/\sigma$, respectively. In the special case when $b$ is held fixed, a more natural definition for those length scales includes $b$ as a prefactor to $\sigma$. We define a shorthand notation for the four possible length scales in Table 1. Their primary purpose is simply to nondimensionalize along-fault distances.

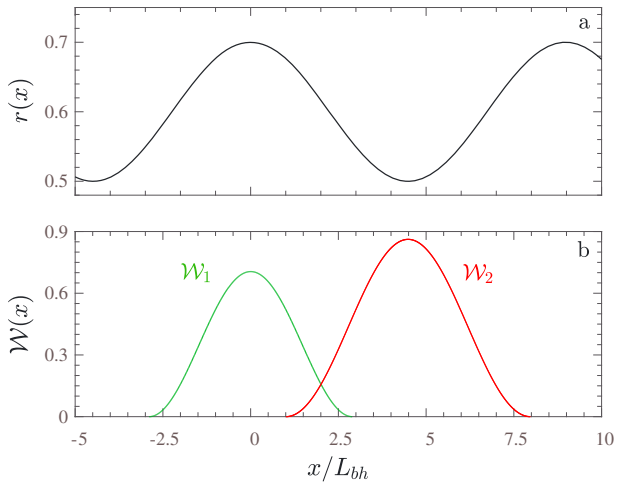


**Figure 2.** The direct effect parameter $a$ is varied, while the evolution effect parameter $b$ is fixed: consequently, the relative rate-weakening magnitude $r = (b - a)/b$ and $m = b - a$ vary in concert. (a) The distribution of the former is shown. (b) We find that two self-similar solutions for slip rate exist on the fault interval considered: the spatial distribution $\mathcal{W}$ of (14) is shown. The length-scale $L_{\mathrm{bh}}$ is defined in Table 1. Here like elsewhere unless otherwise noted, the thin-slab fault model of Figure 1b is considered and results would be qualitatively similar for a model with longer-range of interaction, such as that of Figure 1c. The green and red colors indicate whether the solutions are asymptotically stable, or not, respectively (see also section 6).

We now proceed to obtain solutions of $\mathcal{W}(x)$ for specified distributions of $r(x)$ and $m(x)$. Where results are largely qualitatively independent of the range of elastic interaction, we will focus on the specific results for the thin-slab model. However, when the range of interaction plays a qualitatively determining role, we will highlight the difference.

## 5. Self-Similar Solutions for Diverging Slip Rate Under Frictional Parameter Distributions

Given specific distributions of frictional parameters $a$ and $b$, the function $\mathcal{W}$ determining the distribution of diverging slip rate can be solved for in (24a) or (24b). Because we find that the behavior of solutions under short- and long-ranged elastic interactions are often qualitatively similar, we focus on solutions to the short-ranged problem (24a). In the following, we consider spatial distributions for the parameters $a$ and $b$, expressed as variations of the *relative* and *absolute* magnitudes of steady state rate-weakening $r = (b - a)/b$, and $m = b - a$, respectively. We consider the two quantities to vary in or out of concert, as well as variations occurring over disparate length scales, which includes the possibility that one remains uniformly distributed while the other varies. We find that the self-similar solutions for diverging slip rate, represented by the solution for $\mathcal{W}$, are located around maxima, minima, and in some cases, between the extrema, of the parameter distributions. That these solutions are localized in space indicates a potential for preferential locations for instability development. In the subsequent section, we will demonstrate by analysis that a subset of these solutions can be deemed as favorable to occur, such that we will be able to conclude heterogeneous frictional properties lead to preferential sites for instability development, and ultimately, earthquake nucleation.

### 5.1. Scenarios for Which Locations of Self-Similar Instability Solutions Are Determined by the Distribution of the Relative Magnitude of Steady State Rate Weakening, $r = (b - a)/b$

Here we find the self-similar solutions for diverging slip rate (i.e., distribution $\mathcal{W}$) under arbitrary variations of $r$ and $m$ including the scenarios when (i) $r(x)$ and $m(x)$ vary in concert, such that their maxima and minima coincide; and (ii) $r(x)$ and $m(x)$ vary out of concert (i.e., their distributions are out of phase) and vary over comparable length scales. Solutions are shown for the short-ranged elastic interaction, problem (24a), and are qualitatively similar for the long-range case. Here we find that for scenarios (i) and (ii), the variable relative magnitude of steady state rate weakening, $r$, determines the location $\mathcal{W}(x)$, irrespective of variation of $m(x)$ and the range of elastic interaction. Specifically, we find that $\mathcal{W}(x)$ occurs at maxima and minima of the distribution of $r$.

The rate-weakening magnitudes $m = b - a$ and $r = (b - a)/b$ vary in concert if $a$ varies in space and $b$ remains uniform. In Figure 2a we show the distribution of $r$ and $m$ resulting from one particular choice for the distribution of $a$. In addition to a uniform value of $b$, the normal stress $\sigma$ and slip-weakening distance $D_c$ are also presumed constant and the resultant problem for $\mathcal{W}$ is that of (24a). Numerical solutions of (24a) for $\mathcal{W}$ are shown in Figure 2b. Specifically, we find that a finite number of distributions $\mathcal{W}_i(x)$ (here $i = 1, 2$) exist along an interval of position $x$ along the fault. We note that the (self-similar) solutions $\mathcal{W}_i$ are located about the local maxima and minima of steady state rate weakening. That there are only a finite number $\mathcal{W}_i(x)$ for a finite interval of $x$ of lies in contrast with solutions under uniform properties and normal stress (Rubin & Ampuero, 2005; Viesca, 2016a, 2016b). In this latter case, a self-similar solution $\mathcal{W}$, say, about an origin, could be continuously translated along the fault due to the problem's translational symmetry, implying that a finite interval of distance along the fault hosts an infinite number of self-similar solutions.

We now look to find whether the magnitude or relative magnitude of rate weakening determines the location of the (self-similar) instability solutions $\mathcal{W}_i$. To do so, we explicitly consider a spatial variation of the rate-weakening magnitude $m(x)$ that is phase shifted with respect to the relative magnitude $r(x)$ (Figures 3a and 3c). Both $m$ and $r$ are chosen to vary over similar length scales. The resulting locations for distributions

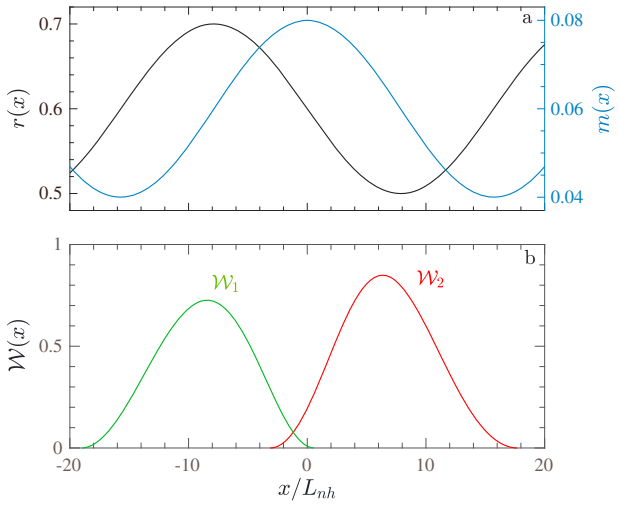


**Figure 3.** (a) We examine the effect of having $m = b - a$ (blue) and $r = (b - a)/b$ (black) vary out of concert with comparable wavelength. (b) We show that the location of the self-similar solutions (14) occurs about the extrema of the distribution of $r$, not those of $m$. The length-scale $L_{\text{nh}}$ is defined in Table 1.

$\mathcal{W}_i$, shown in Figure 3c, coincide with the extremum of $r(x)$, and not those of $m(x)$. Thus, perhaps surprisingly, in this case it is the relative magnitude of steady state rate weakening, and not its magnitude, that determines the location of the self-similar instability solutions.

### 5.2. Scenarios for Which Locations of Self-Similar Instability Solutions Are Determined by the Distribution of the Magnitude of Steady State Rate Weakening, $m = b - a$

We now consider two scenarios for which we find that the magnitude of steady state rate weakening determines the location of the self-similar instability solutions. The scenarios are when the characteristic wavelength of variation of the relative magnitude $r = (b - a)/b$ is much greater or less than the characteristic wavelength of variation of $m = b - a$. Under each scenario, we find that the location $\mathcal{W}$ occurs about extrema of $m$. Additionally, depending upon the rate at which $m(x)$ varies in space, we also find $\mathcal{W}$ occurring between the extrema of $m(x)$ distribution. We first consider the case in which $r$ is uniform and $m$ varies (Figures 4a–4c). Here we find that not only do the self-similar solutions exist about the extrema of $m$ but, as mentioned above, we also find the existence of a solution occurring about the inflection point. On the other hand, we also consider a variation of $r$ that occurs over much shorter wavelengths than those of $m$ (Figures 4d–4f). Here we also find that $m$ determines the location of the self-similar solution and that these solutions again occur about the maxima, minima, and between them.

## 6. Self-Similar Solution Stability and Preferential Locations for Nucleation

In the previous section, we considered spatial variations in frictional parameters and we found the existence of a finite number of solutions for a nonlinear, slip rate instability. These solutions were localized to extrema in variations of steady state rate-weakening parameters and, in one case of parameter variation, to between extrema as well. This raises the question of which, if any, of these solutions may be realized during unstable evolution of slip rate on the fault. Specifically, we are interested to determine whether these solutions may indicate a bias or preference for locations along the fault to host accelerating slip and the eventual nucleation of dynamic rupture. To do so, we will first recast the system of slip rate and state evolution equations to a system that is more amenable to examine instability development. We will find that the solutions for diverging slip rate of the form (14) correspond to fixed points of this new system. Moreover, we can test the attractiveness of these fixed points by performing a linear stability analysis of these fixed points. A fixed point being attractive implies that slip rate, when accelerating unstably, may come to diverge in the fashion of (14) with the distribution $\mathcal{W}$ corresponding to the fixed point. We will find that only a subset of the solutions found in the previous section are attractive and that the location of these attractive places for instability will occur at just one of the following locations: local maxima, minima, or between them.

### 6.1. Reexpressing Evolution Equations to Facilitate Analysis of Instability

Here we reconsider the governing equations for slip rate and state in light of the existence of the self-similar solutions of diverging slip rate. First, we will find an apparent alternative choice for a state variable, one that is not expected to evolve in time when slip rate diverges in the manner of the self-similar solutions. This alternative choice will provide a convenient indication of whether slip rate is close to or far from steady state. Additionally, we will go beyond the ansatz (14) to consider that the spatial distribution may also evolve in time. In doing so we will also find a more convenient choice for the independent variable corresponding to the progression of time. This will ultimately lead to a new pair of evolution equations for which the self-similar solutions are a fixed point. In the subsequent subsections we will examine the stability of these fixed points.

Considering the rate of the friction coefficient (18), the expression (13) resulting from the comparison of strength and stress evolution during an instability, as well as the aging-law expression for state evolution (7),

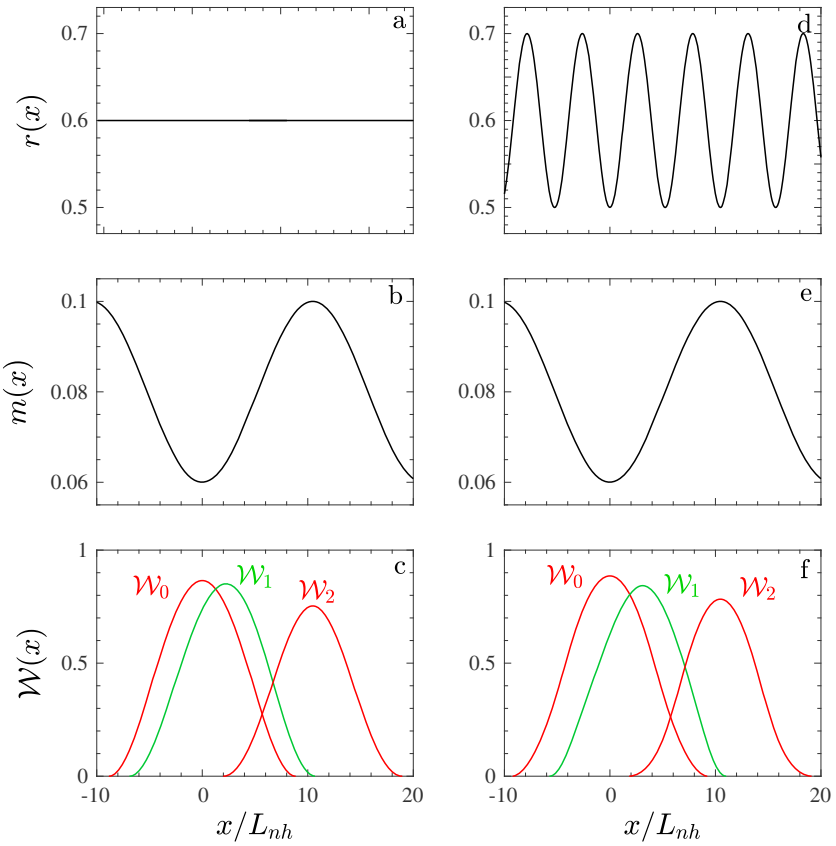


**Figure 4.** (a) We consider cases where $r = (b - a)/b$ varies over two extreme length scales, relative to those over which $m = b - a$ varies. We consider an extreme case where (Figure 4a) $r$ is uniform with (b) $m$ variable for which (c) the self-similar solutions for slip rate instability localize to the critical points of $m$: maxima, minima, and between them. On another extreme, we consider a case where (d) $r$ varies much more rapidly than (e) $m$, again (f) self-similar solutions localize about the critical points of $m$.

we may rearrange to express the evolution equations for slip rate and state as

$$\frac{1}{v(\boldsymbol{x},t)}\frac{\partial v}{\partial t} = \frac{\mathcal{L}[v(\boldsymbol{x},t);\boldsymbol{x}]}{\sigma(\boldsymbol{x})a(\boldsymbol{x})} + \frac{b(\boldsymbol{x})}{a(\boldsymbol{x})}\frac{v(\boldsymbol{x},t)}{D_c(\boldsymbol{x})}\left[1 - \frac{D_c(\boldsymbol{x})}{v(\boldsymbol{x},t)\theta(\boldsymbol{x},t)}\right] \tag{25a}$$

$$\frac{1}{\theta(\boldsymbol{x},t)}\frac{\partial \theta}{\partial t} = -\frac{v(\boldsymbol{x},t)}{D_c(\boldsymbol{x})}\left[1 - \frac{D_c(\boldsymbol{x})}{v(\boldsymbol{x},t)\theta(\boldsymbol{x},t)}\right] \tag{25b}$$

The last quantity in brackets in both expressions is a quantity of interest, which we denote as

$$\Phi(\boldsymbol{x},t) = 1 - \frac{D_c(\boldsymbol{x})}{v(\boldsymbol{x},t)\theta(\boldsymbol{x},t)} \tag{26}$$

Given its definition, we can see that $\Phi$ can be interpreted as a measure of distance from steady state sliding: $\Phi = 0$ for steady state sliding ($v\theta/D_c = 1$) and $\Phi = 1$ when state of the slip is far from steady state ($v\theta/D_c \gg 1$).

We recall that for the self-similar solutions (14) both $v \sim 1/t_f$ and $(\partial\theta/\partial t)/\theta \sim 1/t_f$. Examining the evolution equations (25) with this in mind implies that for these self-similar solutions, $\Phi$ remains constant in time and at most a function of position: that is, $\Phi(\boldsymbol{x},t) = \mathcal{P}(\boldsymbol{x})$. We may determine this function by substituting expressions for $v$ and $(\partial\theta/\partial t)/\theta$ for the self-similar solutions, (14) and (17), respectively, into the above state evolution (25b) equation, from which we find that

$$\mathcal{P}(\boldsymbol{x}) = \begin{cases} 1 & \mathcal{W} \le 1 \\ 1/\mathcal{W}(\boldsymbol{x}) & \mathcal{W} > 1 \end{cases} \tag{27}$$

such that $\mathcal{P}(\boldsymbol{x})$ is determined once $\mathcal{W}(\boldsymbol{x})$ is known.

Apart from the self-similar solutions, however, $\Phi$ will generally evolve in space and time and may be considered as a surrogate for the state variable $\theta$: that is, we may consider the problem of slip rate and state evolution to be posed in terms of the evolution of $v$ and $\Phi$. The pair of evolution equations for that problem follow from substituting $\Phi$ in (25a), and from the definition of $\Phi$ we can deduce that

$$\frac{\partial \Phi}{\partial t} = [1 - \Phi(\boldsymbol{x}, t)] \left[ \frac{\mathcal{L}[v(\boldsymbol{x}, t); \boldsymbol{x}]}{\sigma(\boldsymbol{x}) a(\boldsymbol{x})} + \left( \frac{b(\boldsymbol{x})}{a(\boldsymbol{x})} - 1 \right) \frac{v(\boldsymbol{x}, t)}{D_c(\boldsymbol{x})} \Phi(\boldsymbol{x}, t) \right] \tag{28}$$

We now use the above considerations to examine whether the self-similar solutions are realizable. We begin by relaxing the ansatz (14) such that the spatial distribution of slip rate is now free to evolve with time

$$v(\boldsymbol{x}, t) = \frac{D_c(\boldsymbol{x})}{t_f(t)} W(\boldsymbol{x}, t) \tag{29}$$

We are interested in the evolution of $W$ as $t_f \to 0$, specifically whether $W(x, t) \to \mathcal{W}(x)$. The time derivative of (29) is

$$\frac{\partial v}{\partial t} = \frac{D_c(\boldsymbol{x})}{[t_f(t)]^2} W(\boldsymbol{x}, t) + \frac{D_c(\boldsymbol{x})}{t_f(t)} \frac{\partial W}{\partial t}$$

For both terms to remain comparable requires that $\partial W / \partial t \sim 1 / t_f(t)^{1+\lambda}$ where $\lambda$ is undetermined at this point. This in turn suggests that an appropriate change of independent variable from time $t$ to another variable $s(t)$ is implicitly defined by

$$\frac{\mathrm{d}s}{\mathrm{d}t} = \frac{1}{t_f(t)} \tag{30}$$

such that $s \sim -\log[t_f(t)]$, and $s \to \infty$ as $t_f \to 0$.

This now casts the problem of examining the evolution of slip rate and state during instability development to one of examining the evolution of $W$ and $\Phi$. We carry out the change of independent variable and change our notation $W[\boldsymbol{x}, t(s)]$, $\Phi[\boldsymbol{x}, t(s)] \Rightarrow W(\boldsymbol{x}, s)$, $\Phi(\boldsymbol{x}, s)$. This change of variable transforms the time evolution equations (25a) and (28) for slip rate and $\Phi$ to the pair of evolution equations

$$W(\boldsymbol{x}, s) + \frac{\partial W}{\partial s} = W(\boldsymbol{x}, s) \left[ \frac{\mathcal{L}[D_c(\boldsymbol{x}) W(\boldsymbol{x}, s); \boldsymbol{x}]}{\sigma(\boldsymbol{x}) a(\boldsymbol{x})} + \frac{b(\boldsymbol{x})}{a(\boldsymbol{x})} W(\boldsymbol{x}, s) \Phi(\boldsymbol{x}, s) \right] \tag{31a}$$

$$\frac{\partial \Phi}{\partial s} = [1 - \Phi(\boldsymbol{x}, s)] \left[ \frac{\mathcal{L}[D_c(\boldsymbol{x}) W(\boldsymbol{x}, s); \boldsymbol{x}]}{\sigma(\boldsymbol{x}) a(\boldsymbol{x})} + \left( \frac{b(\boldsymbol{x})}{a(\boldsymbol{x})} - 1 \right) W(\boldsymbol{x}, s) \Phi(\boldsymbol{x}, s) \right] \tag{31b}$$

Fixed points of the evolution equations (31) are solutions for $W$ and $\Phi$ for which $\partial W / \partial s = 0$ and $\partial \Phi / \partial s = 0$. We recall that the self-similar solutions of diverging slip rate correspond to $W(\boldsymbol{x}, s) = \mathcal{W}(\boldsymbol{x})$ and $\Phi(\boldsymbol{x}, s) = \mathcal{P}(\boldsymbol{x})$, such that the self-similar solutions may be identified as fixed points of (31) on this basis alone. Additionally, we recall that $\mathcal{W}(\boldsymbol{x})$ and $\mathcal{P}(\boldsymbol{x})$ are determined by (20) and (27), respectively. We find here that these conditions are equivalent to conditions derived from the evolution equations (31) when looking for solutions for which $\partial W / \partial s = 0$ and $\partial \Phi / \partial s = 0$, that is, solutions $\mathcal{W}(\boldsymbol{x})$ and $\mathcal{P}(\boldsymbol{x})$ satisfying

$$0 = \mathcal{L}[D_c(\boldsymbol{x}) \mathcal{W}(\boldsymbol{x}); \boldsymbol{x}] + \sigma(\boldsymbol{x}) b(\boldsymbol{x}) \mathcal{W}(\boldsymbol{x}) \mathcal{P}(\boldsymbol{x}) - \sigma(\boldsymbol{x}) a(\boldsymbol{x}) \tag{32a}$$

$$0 = [1 - \mathcal{P}(\boldsymbol{x})] [1 - \mathcal{W}(\boldsymbol{x}) \mathcal{P}(\boldsymbol{x})] \tag{32b}$$

Thus, we can now interpret the multiple solutions $\mathcal{W}_i$ obtained in the preceding section as multiple fixed points of (31).

The advantage of considering the pair of evolution equations (31) is that we may now examine the asymptotic stability of the fixed points. A fixed point is said to be linearly stable if small perturbations to $\mathcal{W}$ and $\mathcal{P}$ asymptotically decay as $s \to \infty$ (i.e., as $t_f \to 0$). In the next section, we outline such a stability analysis, which we carry out for the specific fault models and classes of parameter variations considered in section 5.

### 6.2. Stability Analysis of the Self-Similar Solutions

We analyze the stability of the fixed-point solutions by considering perturbations about the fixed points in the form

$$W(\boldsymbol{x}, s) = \mathcal{W}(\boldsymbol{x}) + \epsilon\omega(\boldsymbol{x}, s)$$
$$\Phi(\boldsymbol{x}, s) = \mathcal{P}(\boldsymbol{x}) + \epsilon\phi(\boldsymbol{x}, s)$$

Substituting the above in (31), we arrive to the set of linear evolution equations of $O(\epsilon)$ for the perturbations,

$$\frac{\partial}{\partial s}\begin{bmatrix}\omega\\ \phi\end{bmatrix} = \begin{bmatrix}A_{11} & A_{12}\\ A_{21} & A_{22}\end{bmatrix}\begin{bmatrix}\omega\\ \phi\end{bmatrix} \tag{33}$$

in which

$$A_{11} = \mathcal{W}(\boldsymbol{x})\frac{\mathcal{L}[D_c(\boldsymbol{x})\ *;\boldsymbol{x}]}{\sigma(\boldsymbol{x})a(\boldsymbol{x})} + \frac{b(\boldsymbol{x})}{a(\boldsymbol{x})}\mathcal{W}(\boldsymbol{x})\mathcal{P}(\boldsymbol{x})$$
$$A_{12} = \frac{b(\boldsymbol{x})}{a(\boldsymbol{x})}\mathcal{W}(\boldsymbol{x})^2$$
$$A_{21} = [1 - \mathcal{P}(\boldsymbol{x})]\left[\frac{\mathcal{L}[D_c(\boldsymbol{x})\ *;\boldsymbol{x}]}{\sigma(\boldsymbol{x})a(\boldsymbol{x})} + \frac{b(\boldsymbol{x}) - a(\boldsymbol{x})}{a(\boldsymbol{x})}\mathcal{P}(\boldsymbol{x})\right]$$
$$A_{22} = \frac{b(\boldsymbol{x}) - a(\boldsymbol{x})}{a(\boldsymbol{x})}[1 - \mathcal{P}(\boldsymbol{x})]\mathcal{W}(\boldsymbol{x}) - [1 - \mathcal{W}(\boldsymbol{x})\mathcal{P}(\boldsymbol{x})]$$

To complete the linear stability analysis, we look for solutions $\omega = \omega(\boldsymbol{x})e^{\lambda s}$ and $\phi = \phi(\boldsymbol{x})e^{\lambda s}$. For the fixed-point solutions considered in section 5, we solve the resulting eigenvalue problem numerically by discretizing $\omega(x)$ and $\phi(x)$ along a set of points $x_i$, $i = 1, \ldots, N$ within the domain of $\mathcal{W}(x)$, $\mathcal{P}(x)$, and by solving the resultant matrix eigenvalue problem. Classification of the stability of fixed-point solutions is generally assessed from the sign of the resulting eigenvalues; however, in the subsequent section, we briefly draw attention to a necessary consideration here of a special subset of eigenmodes whose presence is owed to the existence of a temporal or spatial invariance of the governing equations.

### 6.3. Stable, Unstable, and Symmetry Eigenmodes

Generally, a fixed point is said to be asymptotically unstable if there is at least one eigenvalue with positive real part and asymptotically stable if all eigenvalues have negative real parts. Here we highlight that there may exist two modes whose eigenvalues may take on a positive or zero real part but will have no bearing on the assessment of asymptotic stability. Rather, these modes will be a consequence of translational invariance of the governing equations in time or space (e.g., Bernoff et al., 1998). In the problem considered here, however, spatial invariance only occurs when frictional parameters and normal stress are uniform in space (i.e., the cases considered by Rubin and Ampuero, 2005, and Viesca, 2016a, 2016b).

We first consider the invariance with respect to time as a perturbation to the time of instability, $t_{\text{in}}$. Recalling from (30), the time from instability can be written as $t_f = t_c e^{-s}$, where $t_c$ is a time scale set from the arbitrary initial condition for (30). A small perturbation by the amount $\beta t_c$ to the time of instability results in the new time from instability $t_{f,\beta}$ being related to the prior $t_f$ as $t_{f,\beta} = t_f + \beta t_c = t_f[1 + \beta e^s]$ such that

$$v(\boldsymbol{x}, t) = \frac{D_c(\boldsymbol{x})}{t_{f,\beta}(t)}\mathcal{W}(\boldsymbol{x}) = \frac{D_c(\boldsymbol{x})}{t_f(t)}\left[\frac{\mathcal{W}(\boldsymbol{x})}{1 + \beta e^s}\right] \tag{34}$$
$$= \frac{D_c(\boldsymbol{x})}{t_f(t)}\left[\mathcal{W}(\boldsymbol{x}) - \beta\mathcal{W}(\boldsymbol{x})e^s\right] \tag{35}$$

where the last expression follows from an expansion assuming a small perturbation $\beta$. This final expression suggests that a perturbation to the time to instability is represented by eigenmode $w(\boldsymbol{x}) = \mathcal{W}(\boldsymbol{x})$ with a corresponding eigenvalue $\lambda = 1$.

As noted, the existence of a spatial invariance occurs only with no spatial variations in friction parameters or normal stress, for which we can consider perturbations to the location of instability. For small perturbations, the first-order expansion of the distribution $\mathcal{W}$ is

$$\mathcal{W}(\boldsymbol{x} + \boldsymbol{\epsilon}) = \mathcal{W}(\boldsymbol{x}) + \boldsymbol{\epsilon} \cdot \boldsymbol{\nabla}\mathcal{W}(\boldsymbol{x})$$

This is identical to perturbing the fixed-point $\mathcal{W}(\boldsymbol{x})$ with eigenmode $\omega(\boldsymbol{x}) = \epsilon \cdot \boldsymbol{\nabla}\mathcal{W}(\boldsymbol{x})$, or simply $\omega(x) = \mathcal{W}'(x)$ for a single dimension, and eigenvalue $\lambda = 0$. However, introducing heterogeneity in friction parameters removes the invariance of the governing equations to spatial translations, and consequently, corresponding eigenmode can no longer exist. Specifically, under uniform properties a solution for $\mathcal{W}(x)$ could be continuously translated along the fault and remain a solution. In contrast, as shown in section 5, introducing heterogeneity limits solutions to a finite number of distributions of $\mathcal{W}$ at specific locations within a region of the fault dictated by the distribution of parameters. In the next subsection, we examine issues of stability of these remaining fixed points to determine whether they may be considered attractive and asymptotically stable.

### 6.4. Results of Stability Analyses of Considered Scenarios

We apply the stability analysis outlined in the preceding subsection to the self-similar solutions of the type considered in section 5, chiefly involving variations in the magnitude $m$ and relative magnitude $r$ of steady state rate weakening. We begin by briefly reviewing key results of prior work concerning uniform parameter distributions. We then consider in detail the specific cases in which $m$ and $r$ vary in concert as well as when $r$ is fixed and $m$ varies, and we highlight results for other cases. However, generally, we will find that of the self-similar solutions found about the extrema or near inflection points of distributions of $m$ or $r$, only one set will be asymptotically stable, with the remainder being unstable. Thus, we find among these sets of solutions, only one set is indicative of being a preferential nucleation for instability development and earthquake nucleation.

Viesca, (2016a, 2016b) considered the stability of self-similar solutions for the case of uniform frictional parameters and normal stress. The resulting problem reduced to one with a single parameter, $0 < a/b < 1$. A key result was that the self-similar solutions were found to be asymptotically stable below a critical value of $a/b$, the precise value of which is dependent on the specific fault model (i.e., the choice of the operator $\mathcal{L}$). For the short- and long-range interaction models considered here (the thin slab or half-space in contact with another half-space, respectively), those critical values were 0.5 and 0.3781 .... In Figures 5a–5c we show an example self-similar solution for $\mathcal{W}(x)$ and the stability analysis results for the short-range model under uniform parameters and a value of $a/b = 0.3$. We show only the eigenmodes of the stability analysis whose real part is greater than or equal to zero. Here there are two such modes and these modes correspond to those expected given the spatial and temporal invariance of the problem: that is, eigenvalues of $\lambda = 1$ and $\lambda = 0$ and mode shapes proportional to $\mathcal{W}(x)$ and $\mathcal{W}'(x)$, respectively. Thus, we would conclude, in this instance, that the solution for $\mathcal{W}(x)$ is asymptotically stable.

In Figures 5d–5g we consider a perturbation to the uniform case: that is, the case of Figure 2 where $m$ and $r$ vary in concert. For the interval along the fault shown, there exists two self-similar instability solutions about the extrema of $r$ and $m$ (Figure 5e). The stability analysis of the solution located about the maximum of steady state rate-weakening reveals only a single eigenvalue with positive real part, which corresponds to that expected for temporal invariance (Figure 5f). This mode is likewise present when considering the stability of the solution about the minimum (Figure 5g) but is also accompanied by another mode with positive real part, such that this fixed point is asymptotically unstable. While this particular example is for short-ranged elastic interactions, the result for long-range interactions is similar.

We next consider the stability of the self-similar solutions found when $r$ is fixed and $m$ varies (e.g., Figure 4). We found that for this particular case, self-similar solutions existed not only about extrema but also in the intermediate region of inflection points. In examining the stability of these solutions, we will find several remarkable results. First, we find that the stability results vary depending on the nature of the elastic interactions. For short-range interactions, solutions at the maxima of $m$ are always unstable: that is, the regions with the largest magnitude of steady state rate weakening are not attractive locations for instability. Considering the equivalent problem of normal stress variations under uniform $a$, $b$, and $D_c$, this result implies that regions of elevated normal stress are not attractive locations for instability under models such as thin-slab configuration. For long-range interactions, it is the solutions at minima that are always unstable. Second, we find that the solutions about the inflection points do not always exist. Third, the emergence of these inflection point solutions coincides with a change in stability of the solutions occurring about either the minima of $m$ (for short-range interactions) or the maxima (for long range) from stable to unstable.

In Figure 6 we consider the stability of the solutions shown in Figure 4. For each solution, we retrieve the expected eigenmode corresponding to temporal invariance with the eigenvalue $\lambda = 1$. In addition, we find

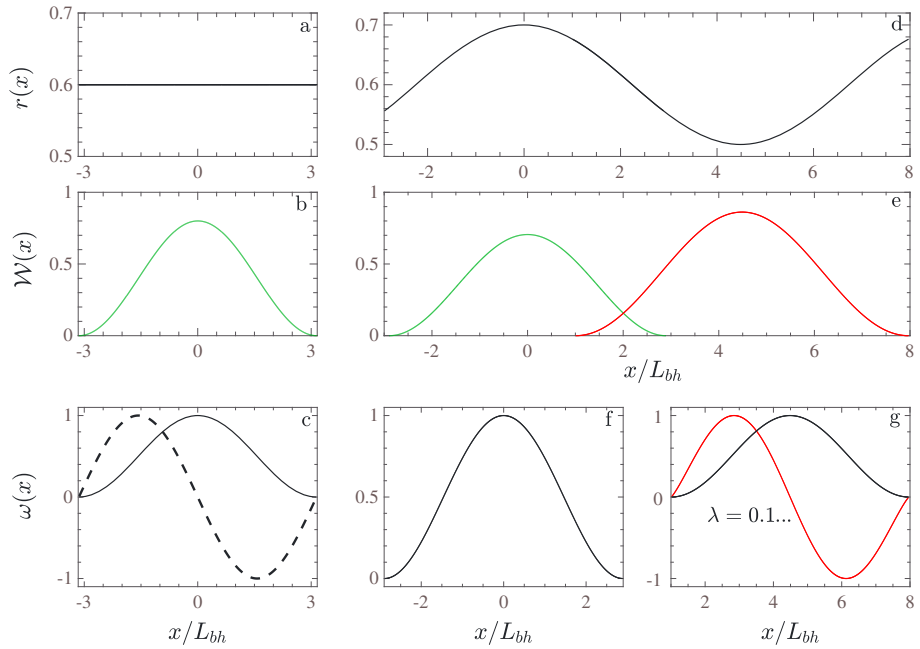


**Figure 5.** Results from linear stability analysis of self-similar solutions for (a–c) spatially uniform values of the direct and evolution effect coefficients $a$ and $b$, and (d–g) variable $a$ and uniform $b$. $a$ and $b$ are chosen such that $r = (b-a)/b = 0.6$ throughout (Figure 5a). The spatial distribution $\mathcal{W}$ for the self-similar solution of the form (14) (Figure 5b). Due to the problem's spatial invariance, this solution may be translated continuously along $x$, though we plot only one solution, centered at $x = 0$. Following the linear stability analysis (Figure 5c) of the solution shown in Figure 5b, we show the eigenmodes whose eigenvalues have a positive or zero real part in Figure 5c. Here the only such eigenmodes are those whose existence is owed to temporal invariance (solid black), for which $\lambda = 1$ and $\omega(x) = \mathcal{W}(x)$ (eigenfunctions are defined within a multiplicative constant) and to spatial invariance (dashed black), for which $\lambda = 0$ and $\omega(x) = \mathcal{W}'(x)$ (within a constant factor). With the absence of any other modes eigenvalues having with positive real part, we find that the self-similar solution represented in Figure 5b is asymptotically stable. For variable $a$ under uniform $b$, the magnitude $m = b - a$ and relative magnitude $r$ of steady state rate weakening vary in concert. The variation of $r$ shown in Figure 5d is that of Figure 2. The break in translational symmetry resulting from the nonuniform distribution of $r$ results in only a finite number of solutions for $\mathcal{W}$, shown in Figure 5e. Likewise, following the linear stability analysis of these solutions, a spatial invariance mode is absent, leaving only the expected temporal invariance mode (black) with $\lambda = 1$ in Figures 5f and 5g where we again plot all modes whose eigenvalues have positive or zero real part. Additionally (Figure 5f), we find that the solution in Figure 5e located about the maximum in $m$ and $r$ (green) has no other mode with positive real part and is therefore asymptotically stable. However (Figure 5g), the solution in Figure 5e, located about the minimum (red), has an antisymmetric mode (red) with positive, real-valued eigenvalue such that the solution is asymptotically unstable. We will color code the asymptotic stability of solutions $\mathcal{W}$ with this green-red scheme throughout.

that the two solutions located about the extrema each has one odd unstable eigenmode and that no unstable modes exist for the solution near the inflection point. Thus, interestingly, we find that for this particular case the solution near the inflection is the only asymptotically stable one and would be expected to be the most attractive location for an instability to develop.

Motivated by the above curious result, we look to further explore the problem of the stability of the self-similar solutions under fixed $r$ and variable $m$. Recalling that the direct and evolution effect coefficients are related to $m$ and $r$ by $a = m(1-r)/r$ and $b = m/r$, the problem (20) determining $\mathcal{W}$ for uniform $\sigma$, $D_c$, and $r$ reduces to

$$\frac{\mathcal{L}[\mathcal{W}(x);x]}{\sigma m(x)/(r D_c)} = \begin{cases} (1-r) - \mathcal{W}(x) & \mathcal{W}(x) \le 1 \\ -r & \mathcal{W}(x) > 1 \end{cases} \tag{36}$$

We consider a periodic variation of $m$ in the form $m(x) = m_o \tilde{m}(x)$, where $m_o$ is the average value of $m$ over the period. Considering the left-hand side of (36), this suggests appropriate length scales of $L_n/m_o$ and $L_{\mathrm{nh}}/\sqrt{m_o}$ for the model faults with long- and short-range interactions, respectively. To develop a low-parameter model for a heterogeneous distribution of $m$, we consider variations of the form

$$m(x) = m_o \left(1 + \alpha \cos\left[\kappa \frac{x}{L_m}\right]\right) \tag{37}$$

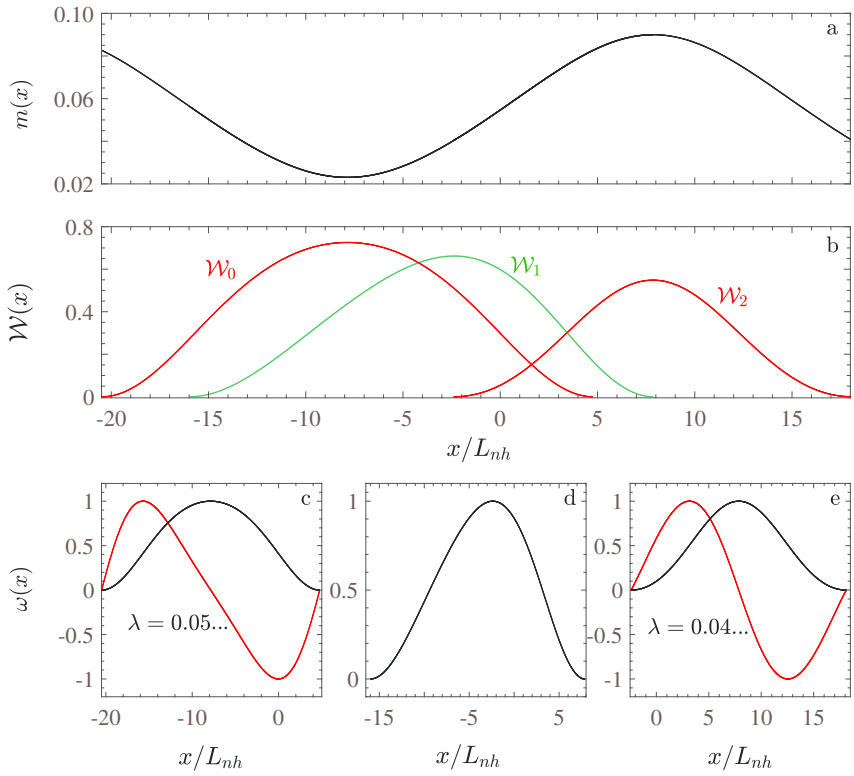


**Figure 6.** Results from linear stability analysis of self-similar solutions found for uniform $r = (b - a)/b = 0.7$, but (a) variable $m = b - a$. (b) The self-similar solutions are found to occur about critical points of the distribution of $m$: the maximum, minimum, and inflection point. Plots of all eigenfunctions whose corresponding eigenvalues have a positive or zero real part for (c) $\mathcal{W}_o$, (d) $\mathcal{W}_1$, and (e) $\mathcal{W}_2$. The stability analysis for the three solutions all shows the presence of the mode owed to temporal invariance (solid black), with $\lambda = 1$. (Figures 6c and 6e) Additionally, the solutions located about the extrema contain one additional unstable eigenmode each (solid red), while Figure 6d the solution about the inflection point contains no such modes and is thus asymptotically unstable.

where $L_m$ stands in for whichever of $L_n/m_o$ or $L_{\mathrm{nh}}/\sqrt{m_o}$ is relevant for the fault model considered. For a given wave number $\kappa$, we study the onset of heterogeneity by increasing $\alpha$ from 0 toward 1.

In Figure 7, we examine the change in stability of the self-similar solutions located about the maximum and minimum of the distributions (37) as $\alpha$ is increased. First, considering the solutions about the maximum, we find that stability is immediately lost as $\alpha$ increases from zero (Figure 7c). The loss occurs as the odd eigenmode corresponding to spatial invariance for the homogeneous case (with $\lambda = 0$ and $\omega(x) = \mathcal{W}'(x)$ for that case) becomes an unstable mode with $\lambda$ increasing from 0 with increasing $\alpha$. In contrast, examining the stability of self-similar solutions about the minimum (Figure 7f), we find that the same invariance eigenmode initially transitions to become a stable mode: that is, $\lambda$ initially decreases from zero with increasing $\alpha$. However, the evolution of $\lambda$ in this case is nonmonotonic and upon further increase of $\alpha$, $\lambda$ becomes positive. Thus, at a critical degree of inhomogeneity $\alpha$, the self-similar solution at the minimum of $m$ loses stability. It is precisely at this moment that the solutions between the extrema of $m(x)$ come into existence. These solutions emerge from the fixed-point solutions at the minimum, and we show their migration in Figure 7h. Owed to the symmetry of the distribution $m(x)$ about the minimum, it is actually a pair of solutions $\mathcal{W}(x)$ that emerge: one migrating leftward, as shown in Figure 7i, and one migrating rightward (not shown). Furthermore, the stability analysis of this symmetric pair of solutions (Figure 7i) shows that they emerge as asymptotically stable solutions, while the solutions about the minimum loses stability. This suggests that bifurcation is a supercritical pitchfork bifurcation. A slight change in the above results occurs when considering long-range elastic interactions: it is the self-similar solutions about the minimum of $m$ which are always unstable for $\alpha > 0$ and the solutions about the maximum go through an interval of stability phase before becoming unstable.

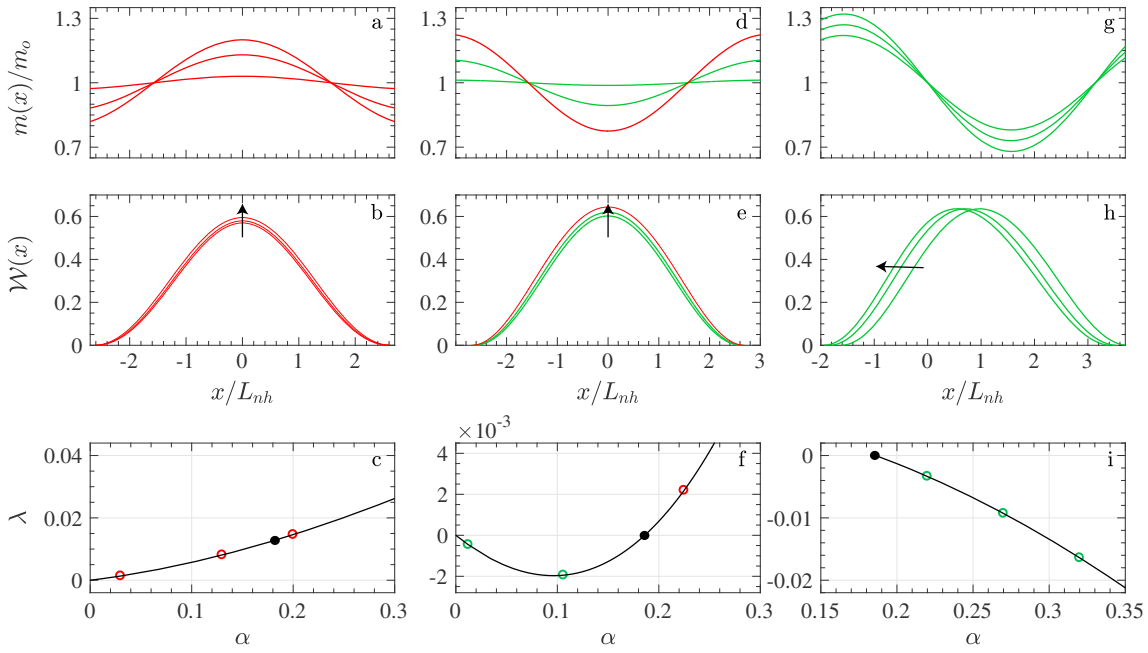


**Figure 7.** Linear stability analysis results for a case in which the degree of parameter heterogeneity is gradually increased with parameter $\alpha$. Here $r$ is uniform and $m$ varies in Figures 7a, 7d, and 7g as (a) $m(x) = m_o[1 - \alpha\cos(x/L_m)]$, (d) $m(x) = m_o[1 + \alpha\cos(x/L_m)]$, and (g) $m(x) = m_o[1 - \alpha\sin(x/L_m)]$ to highlight the behavior, as $\alpha$ is increased, of the self-similar solutions at minima, maxima, and between the extrema, respectively, of the variation (37). The length-scale $L_m = L_{\text{nh}}/\sqrt{m_o}$. (b, e, h) Self-similar solutions for three increasing values of $\alpha$ (arrows indicate sense of increasing $\alpha$). (c, f, i) The eigenvalue trajectory with increasing $\alpha$ for the eigenmode indicative of self-similar solution stability: that is, the eigenmode whose eigenvalue has the greatest real part which is not associated with temporal invariance. In Figures 7c and 7f, when $\alpha = 0$ the eigenmode considered corresponds to the mode due to spatial invariance as both $m$ and $r$ are uniform (for which $\lambda = 0$); with increasing $\alpha$ this mode ultimately becomes an unstable mode, following a stable interval for the case of Figure 7c. Interestingly, as indicated in Figures 7h and 7i, the fixed-point solutions emerge, at a finite value of $\alpha$ corresponding to the point when the fixed-point solution in Figure 7e becomes unstable. Only a leftward propagating set of solutions $\mathcal{W}(x)$ are shown in; however, there exists a rightward propagating set as well (symmetric about minimum of $m$). This, in addition with the stability results, indicates that a symmetrical pitchfork bifurcation occurs at $\alpha = 0.18\ldots$ indicated by the black colored filled circles in Figures 7c, 7f, and 7i.

## 7. Numerical Solutions to Slip Rate and State Initial Value Problems

In section 5 we found that a finite number of self-similar instability solutions exist along an interval of the fault when there is a heterogeneous distribution of frictional parameters. In the preceding section 6, we found that only a subset of these solutions were deemed to be attractive on the basis of a linear stability analysis. In this section, we further demonstrate that such attractive solutions are indeed preferential sites for dynamic rupture nucleation. We find solutions to initial value problems for slip rate and state in which an instability is provoked. We show that the slip rate and state evolves in a manner that asymptotically approaches the attractive fixed-point solutions. This highlights an interesting feature of instability development: that is, the late stage of instability development is independent of the conditions that initiate instability.

We numerically integrate the coupled system of evolution equations for slip rate $v$, (25a), and state $\theta$, (7). We consider simple initial conditions of uniform slip rate and perturbation to the state variable such that sliding is initially at steady state everywhere except within a small region about the origin, where the state variable is initially far from steady state (i.e., the measure $\Phi$ is locally peaked). The normal stress and slip-weakening distance are uniform everywhere, and the frictional parameters $a$ and $b$ are varied via prescribed variations in $m = b - a$ and $r = (b - a)/b$ (Figures 8a and 8c). The system of evolution equations is integrated using an adaptive fourth-order Runge-Kutta method using slip at a point in place of time as the dependent variable to avoid issues of precision as the finite time of instability is approached (as discussed in greater detail in the supporting information of Viesca, 2016a). The spatial discretization is uniform, and the operator $\mathcal{L}[v(x,t);x]$ is evaluated at the collocation points using the discrete Fourier transform and its inverse for both the short- and long-ranged versions of the operator $\mathcal{L}$, (22) and (23), respectively.

In Figures 8 and 8d the evolution of slip rate is shown at snapshots in time for both long- and short-ranged elastic interactions. The qualitative nature of evolution is similar for both types of elasticity, and we present

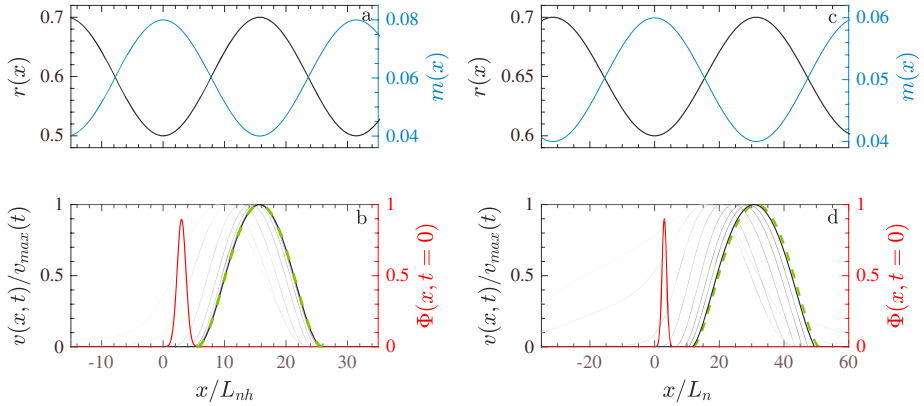


**Figure 8.** Numerical solutions to a slip rate and state initial value problem in which both (a, b) short-range and (c, d) long-range elastic interactions are considered. Slip rate and state evolve on a fault whose frictional properties vary with similar distributions of $m = b - a$ and $r = (b - a)/b$ for each problem and are shown in Figures 8a and 8c. Slip rate evolution at snapshots in time is shown in grey scale (darkening progressing with time) (Figures 8b and 8d); each curve is scaled by its maximum value and is shown at intervals of $v_{max}(t)/v_{init} = 10^{2^n}$ with $n = 1, 2, \ldots, 8$; a slip rate instability is provoked by an initial perturbation to the proximity to steady state $\Phi$ (red); solutions converge to an asymptotically stable self-similar solution (dashed green). Simulations presume quasi-static deformation throughout; however, inertial effects leading to dynamic rupture initiation would be expected to become important somewhere between $n = 3$ and $n = 4$.

them for the sake of completeness. The initial condition $\Phi(x, t = 0)$ is shown by the red peaked curves. The gray curves in the Figures 8b and 8d, which darken progressively to black with time, show the evolution of slip velocity $v(x, t)$, scaled by its maximum value at each snapshot. The dashed green curves are derived from the stable self-similar solutions (and are equal to $\mathcal{W}(x)/\max[\mathcal{W}(x)]$). Clearly, the quasi-static acceleration of slip rate becomes independent of the imposed initial condition, coinciding with the behavior of the stable self-similar solution. We also note that the slip rate evolved away from the minimum of $r(x)$, where there exists an unstable fixed-point solution, which here also corresponds to the minimum of $m$ (i.e., the region of strongest rate weakening). Although the asymptotic evolution of slip rate is indeed self-similar and independent of the initial condition and external forcing, when multiple attractors are present (periodically so here), the slip rate evolution will be biased toward one depending on initial conditions and external forcing.

## 8. Discussion

We apply the analyses of the preceding sections to consider three problems in further detail. First, we consider the typical depth distribution of frictional parameters assumed in seismic cycles and show that several model results can be anticipated on the basis of the frictional property distribution alone. Second, we examine the question of what is the minimum size of a rate-weakening region that can support instability. We illustrate results when a rate-weakening patch is embedded within a rate-strengthening region and show that the rate-strengthening region may participate in unstable acceleration. Last, we touch upon the role played by the characteristic length scale over which frictional properties vary, relative to the size of the fault area over which an instability develops.

### 8.1. Implications for Earthquake Nucleation in Seismic Cycle Models

We examine the depth distribution of frictional properties typically assumed in models of the seismic cycle and, on this basis, show that the nucleation behavior observed in these models may be anticipated. We also highlight how perturbations to the depth distribution may manifest itself in altered behavior in the earthquake nucleation models.

Tse and Rice (1986), following experimental results of Stesky (1975), Dieterich (1981), and Tullis and Weeks (1986), presumed a depth dependence of frictional properties in which a transition from rate weakening to rate strengthening occurred at depth and used this dependence to formulate a model for the earthquake cycle (schematically shown in Figure 9a), in which steady fault creep at depth drives the intermittent dynamic rupture of the rate-weakening interval. Such a depth dependence was further bolstered by experiments under

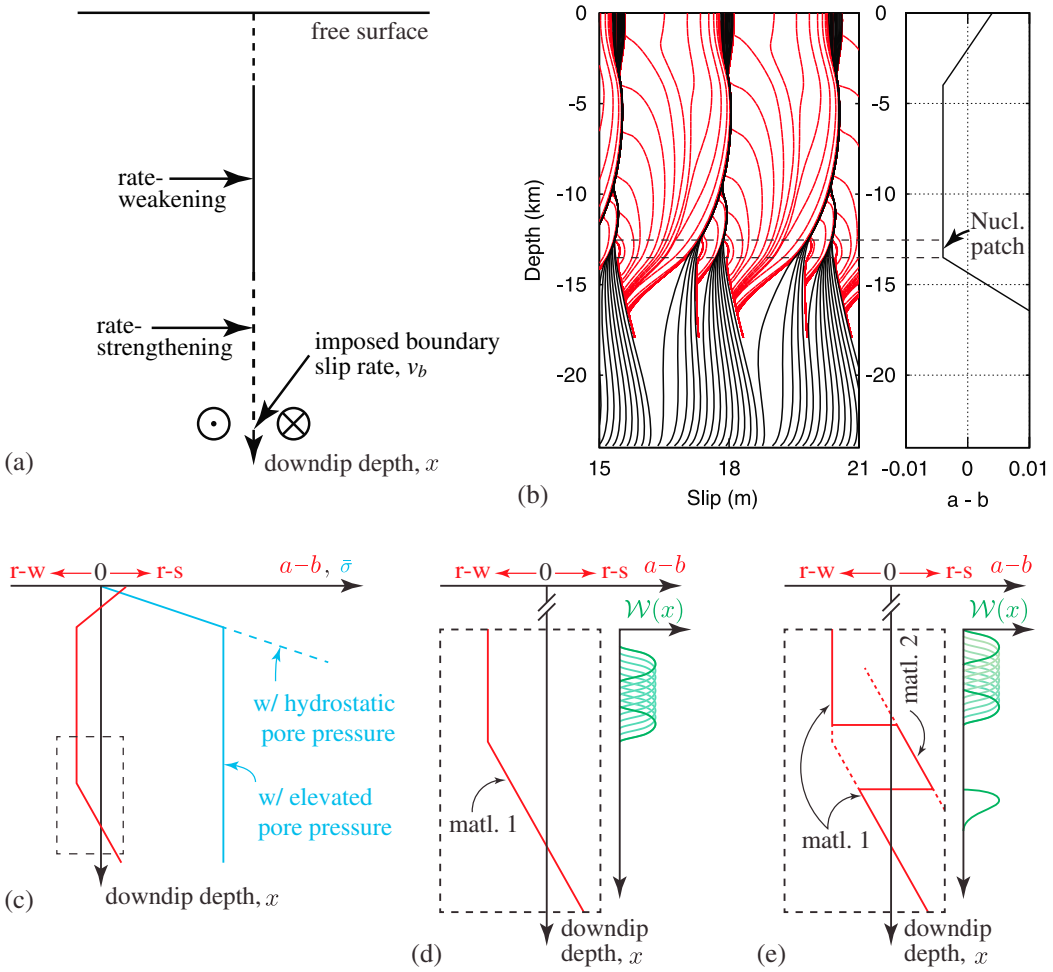


**Figure 9.** (a) Schematic of depth dependence of frictional properties and boundary conditions for two-dimensional, antiplane earthquake cycle models. (b) Model results of Lapusta and Rice (2003) showing (left) slip distribution in time with black contours plotted at 5 year intervals during an interseismic period, and red contours plotted at 5 s intervals during a coseismic period; and (right) the depth dependence of the steady state rate-dependence $a - b$ used in the model. For the interval shown $a = 0.15$ while $b$ varies, implying both $m$ and $r$ vary in concert. The lower black dashed line indicates the location of the kink in the distribution of $a - b$. The upper black line is a distance $2L$ above where $2L$ is the expected nucleation size on the basis of the analysis for nucleation under homogeneous properties (e.g., Rubin & Ampueno, 2005; Viesca, 2016a) given the homogeneous values of $\sigma$, $D_c$, $a$, and $b$ in that region. Remarkably, the interval bounded by the dashed lines corresponds to the observed nucleation size in the numerical solutions. (c) Schematic plot of both steady state frictional properties and effective normal stress frequently used in seismic cycle models. (d) Examining depth distributions of the type in Figure 9c, with uniform effective normal stress, via the analysis of this paper shows no instability solutions exist in the linear transition region. Rather, the uniform distribution of the rate-weakening plateau implies the existence of a spatially translatable solution there. (e) Schematic of a simple perturbation, in which the principal gouge compositions changes with depth between two materials, each with its own depth dependence for $a-b$. The solid red line indicates the depth distribution of $a-b$. An interruption of the gouge composition, from material 1 to material 2, permits a preferential nucleation site on the lower sloped region. The dashed red lines indicate what would be the depth distribution of $a - b$ had the gouge been principally composed of material 1 or 2 at a given depth.

representative pressure and hydrothermal conditions (e.g., Blanpied et al., 1991, 1995, 1998; He et al., 2007) and has continued to be incorporated in seismic cycle models since (e.g., Lapusta et al., 2000; Rice, 1993).

A recurring feature in these models is that the rate-weakening interval is dominated by uniform frictional properties, represented by a plateau in the distribution in Figures 9b and 9c, with a linear transition to rate-strengthening occurring at depth. Additionally, it is often the case that the effective normal stress is taken to be approximately uniform over the same interval, possibly owing to elevated fault zone pore fluid pressures (e.g., Rice, 1992). While these choices may also have been partly made for model simplicity, we find that this has a consequence of permitting the existence of a continuously translatable solution for $\mathcal{W}(x)$: that is, there

are an infinite number of locations along the plateau this interval that are potentially attractive for the nucleation of an earthquake (Figure 9d). As seen in the results of Lapusta and Rice (2003) shown in Figure 9b, only one (or, in other instances, a small subset) of these locations is chosen due to bias provided by the manner of external forcing.

However, on the basis of our analysis, this sensitivity to the external forcing and the potential variability for earthquake nucleation locations is expected to be reduced or altogether eliminated under somewhat generic adjustments to the depth dependence. One possibility is a profile like that of Figure 9a, however, under a smoother distribution (e.g., continuous in the first derivative with a unique minimum). Such distributions will have a global maximum in rate weakening and will admit a single-instability solution about that maximum. In this case, there is a single location on the fault to which, under quasi-static conditions, a developing instability will asymptotically approach. While inertial effects do not permit the continued acceleration of a location on the fault, such a global maxima will nonetheless provide a persistent bias for the location of nucleation. Another possibility is that there remains an interval of rate weakening, but the distribution is less smooth and more reminiscent of that in Figure 2, in which multiple, locally attractive nucleation sites may occur about local maxima. In this case, a finite number of nucleation sites occur and that of any given site will determine the location nucleation will itself be determined by both the external forcing and history of sliding. Nonetheless, a correlation of earthquake nucleation locations and the distribution of rate-weakening properties would be expected. To highlight how our analysis would inform another model distribution, we consider a specific example scenario sketched in Figure 9e. Here we consider that the principal fault gouge composition alternates between two materials, each with its own temperature (and hence, depth) dependence of $a$ and $b$. Here the alternation is such that a rate-weakening interval is interrupted by a rate-strengthening patch. The existence of this rate-strengthening patch permits the existence of a solution for $\mathcal{W}(x)$ (and hence, a preferential nucleation site) on the remaining sloped rate-weakening transition region at depth. This simple example is one of many conceivable; however, the key result here is that we provide a framework to determine the potential nucleation sites resulting from a given distribution of frictional properties and normal stress.

### 8.2. Minimum Size of Rate-Weakening Region That Can Nucleate an Instability

We now apply the analyses of the preceding sections to the problem of establishing what is the minimum size of a rate-weakening patch that may permit unstable acceleration of fault slip. The interest in such a minimum size is to establish the existence of a critical length scale that characterizes qualitative changes in the nature of accelerating slip, if any, on a fault containing a rate-weakening patch. Specifically, we look toward the existence and type of self-similar instability solutions as an indication whether the spontaneous nucleation of seismicity may transition toward the nucleation of small dissimilar earthquakes, elevated but aseismic slip rates, or steady creep, as the size of the rate-weakening patch is reduced in comparison with the critical length scale.

A first estimate of such a minimum rate-weakening patch size is the critical wavelength $\lambda_{cr}$ found by linear stability analysis of a uniformly rate-weakening interface. The critical wavelength is that which separates whether perturbations grow at wavelengths larger than the critical or decay for those smaller (e.g., Rice & Ruina, 1983; Rice et al., 2001). The wavelength depends on the nature of the elastic interactions and is given by $\lambda_{cr} = 2\pi L_{bh}/\sqrt{1-a/b}$ and $\lambda_{cr} = \pi L_b/(1-a/b)$ for the thin-slab and contacting-half-spaces configuration, respectively (e.g., Lipovsky & Dunham, 2017; Rice & Ruina, 1983; Viesca, 2016a). However, while a convenient first estimate, this neglects the heterogeneity of frictional properties and the nonlinearity of the governing equations. Skarbek et al. (2012) improved on the homogeneous fault representation by modeling a fault with both rate-weakening and rate-strengthening regions as a pair of coupled spring-block sliders, each sliding on either a rate-strengthening or rate-weakening surface, and performed a linear analysis of steady-sliding stability to estimate an alternative critical wavelength.

Our results on self-similar instability solutions and their attractiveness provide a means of establishing a minimum that respects both the inherent problem nonlinearity and frictional property distributions. While the specific examples considered in the preceding sections focused on variable but strictly rate-weakening ($a < b$) properties, the analysis readily extends to distributions with transitions between rate-weakening and rate-strengthening ($a > b$) behavior. We consider the problem of a rate-weakening patch embedded within a rate-strengthening region. In addition to crustal-scale seismic cycle models, such configurations appear, for example, in models of problems ranging from repeating microseismicity (e.g., Chen & Lapusta, 2009),

to spontaneous emergence of slow slip events (e.g., Liu & Rice, 2005), to stick-slip behavior of ice streams (e.g., Lipovsky & Dunham, 2017).

We look to establish the minimum size of a rate-weakening patch that permits the existence of a self-similar solution, and whether that solution is asymptotically stable. We consider the thin-slab fault model and a distribution of frictional properties, in which a rate-weakening patch of width $w$, with uniform values of $a$ and $b$, is embedded within an outer rate-strengthening region, also with uniform values of $a$ and $b$. We are interested in the minimum value of the width $w$ that admits a self-similar instability solution, $w_{\text{min}}$. If the outer region is rate neutral such that $(a/b)_{\text{out}} = 1$, we find a closed form expression for $w_{\text{min}}$: $w_{\text{min}} = 2L_{\text{bh}}/[1 - (a/b)_{\text{in}}]$, where $0 < (a/b)_{\text{in}} < 1$ is the ratio of $a$ and $b$ in the rate-weakening patch. Comparing this $w_{\text{min}}$ with the critical wavelength $\lambda_{\text{cr}}$ from the linear stability analysis corresponding to the thin-slab problem, we find that $w_{\text{min}}$ remains below $\lambda_{cr}$, evaluated using $(a/b)_{\text{in}}$, for most values of $(a/b)_{\text{in}}$. Finding the minimum width $w_{\text{min}}$ under arbitrary choices of the pair of parameters $(a/b)_{\text{out}} > 1$ and $0 < (a/b)_{\text{in}} < 1$ is outside the scope of the present discussion; however, the expression for $w_{\text{min}}$ for a rate-neutral exterior region can be considered a lower bound. We may also examine the more general problem of finding $\mathcal{W}(x)$ given $(a/b)_{\text{in}}$, $(a/b)_{\text{out}}$, and $w$. In Figure 10d, we highlight a specific example of a distribution in which $(a/b)_{\text{out}} = 1.2$, $(a/b)_{\text{in}} = 0.3$ and $w = w_{\text{min}}(\approx 3.16L_{\text{bh}})$. In Figure 10e, we plot the solution for $\mathcal{W}(x)$ given this distribution. Interestingly, we find in this case that $\mathcal{W}(x)$ extends into the rate-strengthening region (i.e., $2L > w$): the self-similar solution indicates that the rate-strengthening region participates in the unstable acceleration of slip. If $w$ is decreased below $w_{\text{min}}$, while $(a/b)_{\text{out}}$ and $(a/b)_{\text{in}}$ remain constant, there would no longer exist a solution for $\mathcal{W}(x)$. If $w$ is increased, we would eventually find solutions where $\mathcal{W}(x)$ is wholly supported within the rate-weakening region (i.e., $2L \leq w$). The point at which this transitions occurs is when $w$ reaches the value of $2L$ given by the solution for $\mathcal{W}(x)$ under a homogeneous distribution of frictional parameters with the ratio $(a/b)_{\text{in}}$ (i.e., the problem considered by Rubin and Ampuero, 2005; Viesca, 2016a, 2016b).

If rate-weakening patches exist, then the above results present three possible scenarios. One scenario is shown in Figure 10a, in which the rate-weakening patch size is greater than the nucleation patch size (i.e., corresponding to the case $2L < w$ in the thin-slab example above). In this scenario slip instability may give way to a dynamic rupture that can propagate across the rate-weakening patch, and beyond if there is a transition from rate-strengthening to weakening at coseismic slip rates, or if the density of rate-weakening asperities is sufficiently large (e.g., Dublanchet et al., 2013). In this scenario, nucleation requires only small perturbation for $w$ sufficiently large. A second scenario is shown in Figure 10b, in which the rate-weakening patch size is less than the extent of the instability solution (i.e., $w < 2L$ in the thin-slab example). Here slip instability may give way to dynamic rupture, which will quickly dampen unless coseismic weakening mechanisms are triggered. Such behavior might appear as a triggered aseismic slip event or a dynamic rupture that radiates dissimilarly to events with a larger runout distance, with different characteristic initial and stopping phases. For nucleation patch size to extend beyond the rate-weakening patch implies that the rate-weakening patch is marginally unstable: that is, for the thin-slab example, this corresponds to $w$ approaching $w_{\text{min}}$, which is expected to be less than $\lambda_{\text{cr}}$ from the stability analysis of steady sliding to infinitesimal perturbations. This suggests that finite perturbations may be required to initiate a slip instability in this case. A third scenario is when the rate-weakening patch size is so small that no self-similar solutions exist. This likely implies that the rate-weakening patch will be slaved to the sliding surrounding rate-strengthening and undergo stable, near-uniform creep.

### 8.3. Length Scales of Nucleation and Parameter Variation

The length scale(s) over which frictional properties vary and the extent of the fault that an instability solution occupies are independent quantities and their ratio is a problem parameter. The former may be determined, for example, by variations in temperature and fault gouge composition, while the latter has a characteristic length scale of the type found in Table 1. In the examples of property distributions considered in sections 5–7, for which we found solutions for self-similar instability and their stability, the rate of variation of frictional properties was comparable to the self-similar solutions' along-fault extent (i.e., the distance $L$ for the examples considered). Here we briefly discuss circumstances in which the two quantities may be disparate and the implications for instability development.

On one hand, variations on the crustal scale, as discussed in subsection 8.1, provide sufficient heterogeneity for seismic cycle models while the nucleating patch size may be expected to be much smaller—on the meter to tens-of-meters scale, owing, for example, to small, μm-to-mm-scale values of the characteristic slip

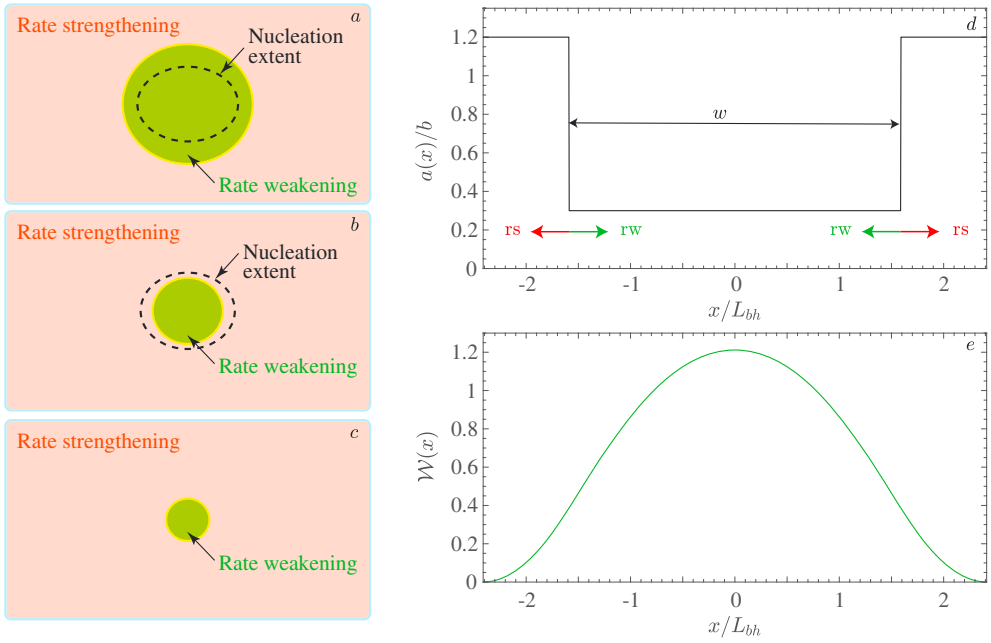


**Figure 10.** (a–c) Schematic of steady state velocity-weakening patch of varying sizes in a velocity-strengthening region. (a) Rate-weakening patch is large enough such that the self-similar instability solution occurs within the rate-weakening domain (Figure 10a). Size of velocity-weakening patch is just large enough to admit a self-similar instability solution, whose boundary is denoted by a dashed curve, which may extend into the rate-strengthening region (Figure 10b). The rate-weakening patch size may be smaller than a critical patch size expected from a linear stability analysis, implying that instability development in this case may require a finite perturbation. In the absence of engagement of strong weakening at the elevated slip rates instability about the rate-weakening patch would give rise to a slow or a subdued dynamic slip event in the surrounding rate-strengthening region. Size of velocity-weakening patch is sufficiently small such that no self-similar instability solution exist (Figure 10c). (d, e) An in-plane or antiplane example of the situation in Figure 10b. The distribution of $a(x)/b$ is given in Figure 10d and the corresponding solution of $\mathcal{W}(x)$ in Figure 10e. The solution is asymptotically stable. The size of the rate-weakening patch is the smallest possible for a stable fixed-point solution, given the inner and outer values of $a/b$.

distance $D_c$. If property variations occur only on the crustal scale, large swaths of the fault might appear as nearly homogeneous such that the results of Rubin and Ampuero (2005) and Viesca, (2016a, 2016b) apply (as indicated by the spacing of the black-dashed lines in Figure 9b). However, as noted in the previous subsection, the manner of crustal-scale variations may still play a determining role in the location of earthquake nucleation in the models. Furthermore, our results highlight the costs of homogenizing for model simplification purposes, or otherwise neglecting, what in reality may be a more heterogeneous distribution. Under homogeneous properties, spatial invariance leads to an infinite number of potential locations for instability to develop whereas heterogeneous properties, even within entirely rate-weakening regions, provide a countable number of preferential nucleation locations.

On the other hand, there are conditions in which the nucleating patch size may be larger than the scale over which properties vary. Given that the expected nucleation patch size is inversely proportional to the effective normal stress, one such condition is when fault pore fluid pressures reach near-lithostatic values. Indications for such follow from models of fault zone fluid flow or mineral dehydration in subduction zones, as well as from seismological observations and inversion of models of slow slip (e.g., Audet et al., 2009; Liu & Rice, 2007; Rice, 1992; Saffer & Tobin, 2011). When the self-similar solution length scale is much larger than that characterizing, say the variation of $a - b$, a self-similar solution will encompass several maxima and minima of the distribution. When the number of encompassed extrema are large, a large number of instability solutions exist, each separated only by a small shift relative to its extent. Thus, while explicit consideration of the heterogeneity removes a spatial invariance, a discrete but near-continuous translatability of instability solutions is retrieved when the length-scale disparity is great. in this case, there may no longer be a reliable prediction as to preferential location of instability.

This scenario is examinable with the model property distribution of (37). Specifically, we may start with a finite value of $\alpha$ but infinitesimal value of $\kappa$ such that the distribution is nearly homogeneous. Taking $\kappa$ as a problem parameter, which implicitly compares the wavelength of variation to the length-scale $L_m$ and has a larger range to explore heterogeneity than $\alpha$, we may examine the behavior in the limit $\kappa \to \infty$. Doing so, we retrieve the initial pitchfork bifurcation of the type seen in Figure 7 at a finite value of $\kappa$. As $\kappa$ is increased, this bifurcation is followed by a localization of self-similar solutions centers to maxima and minima of $a-b$, as well as an alternation of their stability as a series of transcritical bifurcations. We leave a more detailed discussion of such a scenario for later work.

## 9. Summary and Conclusion

A number of observations point toward a likely variation of fault frictional properties and normal stress, both downdip and along strike. Considering a slip rate- and state-dependent description of the frictional strength of a fault within an elastic continuum, we examine the nonlinear spatiotemporal development of a slip rate instability under heterogeneous frictional properties and normal stress. Such instabilities are thought to nucleate the earthquake-generating dynamic rupture of faults. We find the existence of self-similar solutions of a slip rate instability that are determined by the frictional parameter and normal stress distributions, as well as the details of the setting of the slip surface within the elastic medium, but are otherwise independent of initial conditions and external forcing. We find that the problem determining these solutions is equivalent to that determining the distribution of slip for a crack with a piecewise-linear slip-weakening friction coefficient in equilibrium with a given stress state, in which the fault shear and normal stresses, as well as the peak and residual levels of the friction coefficient and characteristic slip distance, are heterogeneous in space.

We further examine the particular case of variations in parameters controlling the local steady state rate-weakening behavior of the fault: the direct and evolution effect coefficients $a$ and $b$. We consider variations in the magnitude of steady state rate weakening, $m = b - a$, as well as the relative magnitude $r = (b-a)/b$. While attention is explicitly given to the consequence of spatial distributions of this parameter pair, with the normal stress $\sigma$ and critical slip distance for state evolution $D_c$ remaining uniform, we find that particular variations of $a$ and $b$ are equivalent to the variations in $\sigma$ or $D_c$, such that results presented here can be implicitly extended to evaluate such cases. For instance, variations in $m$ with uniform $r$ correspond to variations $\sigma$ under uniform values of $a$, $b$, and $D_c$. Under the prescribed variations of $m$ and $r$, we solve for the self-similar solutions. When frictional parameters or normal stress vary, only a finite number of self-similar solutions exist. For the cases considered, we find that the solutions are localized to extrema, and in some cases between the extrema, of the distributions of $m$ and $r$, determined partly by the relative distances over which the quantities vary.

While we find that a number of self-similar solutions exist intermittently along the fault, we consider whether any of these solutions are attractive, and hence, a preferential site for earthquake nucleation. Specifically, we first reformulate the problem for slip rate and state evolution as that of a dynamical system in which the self-similar solutions are fixed points. Subsequently, we perform a linear stability analysis to assess whether the fixed points are asymptotically stable (and consequently, attractive) or unstable (relatively unattractive). We find that only a subset of solutions are attractive (e.g., those occurring about a coincidental maxima of $r$ and $m$, when those quantities vary in concert), with the other set (e.g., those about the coincidental minima of $r$ and $m$) being unstable. That only a finite number of attractive instability solutions exist intermittently along the fault lies in contrast to the case when all parameters are held uniform. In the uniform case, an attractive self-similar solution may be continuously translated along the fault, such that while the structure of the solution remains the same, the particular location of instability is not determined a priori. In this case, while the asymptotic behavior of the instability may be determined by the self-similar solution, the particular location is determined by details of the initial condition and external forcing. However, we find that when properties vary in space both the asymptotic acceleration of the slip rate and the location of that acceleration on the fault is determined a priori by the heterogeneous distribution of parameters.

**Acknowledgments**
This study was supported by NSF-EAR award 1344993 and by the Southern California Earthquake Center (SCEC), funded by NSF Cooperative Agreement EAR-1033462 and USGS Cooperative Agreement G12AC20038. This is SCEC contribution # 7927. R. C. Viesca is also grateful for support as a Professeur Invité at the Institut de Physique du Globe de Paris. The authors are thankful to Jean-Paul Ampuero for a detailed review, an anonymous reviewer for comments, and Eric M. Dunham for discussion. No data was used in producing this manuscript.

## References

Ampuero, J.-P., & Rubin, A. M. (2008). Earthquake nucleation on rate and state faults – Aging and slip laws. *Journal of Geophysical Research*, *113*, B01302. https://doi.org/10.1029/2007JB005082

Audet, P., Bostock, M. G., Christensen, N. I., & Peacock, S. M. (2009). Seismic evidence for overpressured subducted oceanic crust and megathrust fault sealing. *Nature*, *457*(7225), 76–78. https://doi.org/10.1038/nature07650

Barbot, S., Lapusta, N., & Avouac, J.-P. (2012). Under the hood of the earthquake machine: Toward predictive modeling of the seismic cycle. *Science*, *336*(6082), 707–710. https://doi.org/10.1126/science.1218796

Baumberger, T., Berthoud, P., & Caroli, C. (1999). Physical analysis of the state- and rate-dependent friction law: II. Dynamic friction. *Physical Review B: Condensed Matter*, *60*, 3928–3939. https://doi.org/10.1103/PhysRevB.60.3928

Bernoff, A. J., Bertozzi, A. L., & Witelski, T. P. (1998). Axisymmetric surface diffusion: Dynamics and stability of self-similar pinchoff. *Journal of Statistical Physics*, *93*(3), 725–776. https://doi.org/10.1023/B:JOSS.0000033251.81126.af

Bilby, B. A., & Eshelby, J. D. (1968). Dislocations and the theory of fracture. In H. Liebowitz (Ed.), *Fracture* (Chap. 2, Vol. 1, pp. 99–182). New York: Academic Press.

Blanpied, M. L., Lockner, D. A., & Byerlee, J. D. (1991). Fault stability inferred from granite sliding experiments at hydrothermal conditions. *Geophysical Research Letters*, *18*(4), 609–612. https://doi.org/10.1029/91GL00469

Blanpied, M. L., Lockner, D. A., & Byerlee, J. D. (1995). Frictional slip of granite at hydrothermal conditions. *Journal of Geophysical Research*, *100*(B7), 13,045–13,064. https://doi.org/10.1029/95JB00862

Blanpied, M. L., Marone, C. J., Lockner, D. A., Byerlee, J. D., & King, D. P. (1998). Quantitative measure of the variation in fault rheology due to fluid-rock interactions. *Journal of Geophysical Research*, *103*, 9691–9712. https://doi.org/10.1029/98JB00162

Brechet, Y., & Estrin, Y. (1994). The effect of strain rate sensitivity on dynamic friction of metals. *Scripta Metallurgica et Materialia*, *30*(11), 1449–1454. https://doi.org/10.1016/0956-716X(94)90244-5

Carpenter, B. M., Scuderi, M. M., Collettini, C., & Marone, C. (2014). Frictional heterogeneities on carbonate-bearing normal faults: Insights from the Monte Maggio Fault, Italy. *Journal of Geophysical Research: Solid Earth*, *119*, 9062–9076. https://doi.org/10.1002/2014JB011337

Chen, T., & Lapusta, N. (2009). Scaling of small repeating earthquakes explained by interaction of seismic and aseismic slip in a rate and state fault model. *Journal of Geophysical Research*, *114*, B01311. https://doi.org/10.1029/2008JB005749

Chlieh, M., Avouac, J.-P., Sieh, K., Natawidjaja, D. H., & Galetzka, J. (2008). Heterogeneous coupling of the Sumatran megathrust constrained by geodetic and paleogeodetic measurements. *Journal of Geophysical Research*, *113*, B05305. https://doi.org/10.1029/2007JB004981

Collettini, C., Niemeijer, A., Viti, C., & Marone, C. (2009). Fault zone fabric and fault weakness. *Nature*, *462*(7275), 907–910. https://doi.org/10.1038/nature08585

Dieterich, J. H. (1978). Time-dependent friction and the mechanics of stick-slip. *Pure and Applied Geophysics*, *116*(4), 790–806. https://doi.org/10.1007/BF00876539

Dieterich, J. H. (1979). Modeling of rock friction: 1. Experimental results and constitutive equations. *Journal of Geophysical Research*, *84*(B5), 2161–2168. https://doi.org/10.1029/JB084iB05p02161

Dieterich, J. H. (1981). Potential for geophysical experiments in large scale tests. *Geophysical Research Letters*, *8*(7), 653–656. https://doi.org/10.1029/GL008i007p00653

Dieterich, J. H. (1992). Earthquake nucleation on faults with rate-and state-dependent strength. *Tectonophysics*, *211*(1), 115–134. https://doi.org/10.1016/0040-1951(92)90055-B

Dublanchet, P., Bernard, P., & Favreau, P. (2013). Interactions and triggering in a 3-D rate-and-state asperity model. *Journal of Geophysical Research: Solid Earth*, *118*, 2225–2245. https://doi.org/10.1002/jgrb.50187

Evans, J. P., & Chester, F. M. (1995). Fluid-rock interaction in faults of the San Andreas system: Inferences from San Gabriel fault rock geochemistry and microstructures. *Journal of Geophysical Research*, *100*, 13,007–13,020. https://doi.org/10.1029/94JB02625

He, C., Wang, Z., & Yao, W. (2007). Frictional sliding of gabbro gouge under hydrothermal conditions. *Tectonophysics*, *445*(3), 353–362. https://doi.org/10.1016/j.tecto.2007.09.008

Head, A. K. (1953). Edge dislocations in inhomogeneous media. *Proceedings of the Physical Society. Section B*, *66*(9), 793.

Heslot, F., Baumberger, T., Perrin, B., Caroli, B., & Caroli, C. (1994). Creep, stick-slip, and dry-friction dynamics: Experiments and a heuristic model. *Physical Review E*, *49*, 4973–4988. https://doi.org/10.1103/PhysRevE.49.4973

Hillers, G., Ben-Zion, Y., & Mai, P. M. (2006). Seismicity on a fault controlled by rate- and state-dependent friction with spatial variations of the critical slip distance. *Journal of Geophysical Research*, *111*, B01403. https://doi.org/10.1029/2005JB003859

Hillers, G., Mai, P. M., Ben-Zion, Y., & Ampuero, J.-P. (2007). Statistical properties of seismicity of fault zones at different evolutionary stages. *Geophysical Journal International*, *169*(2), 515–533. https://doi.org/10.1111/j. 1365-246X.2006.03275.x

Horowitz, F. G., & Ruina, A. (1989). Slip patterns in a spatially homogeneous fault model. *Journal of Geophysical Research*, *94*(B8), 10,279–10,298. https://doi.org/10.1029/JB094iB08p10279

Ikari, M. J., Carpenter, B. M., Kopf, A. J., & Marone, C. (2014). Frictional strength, rate-dependence, and healing in DFDP-1 borehole samples from the Alpine Fault, New Zealand. *Tectonophysics*, *630*, 1–8. https://doi.org/10.1016/j.tecto.2014.05.005

Jolivet, R., Lasserre, C., Doin, M.-P., Peltzer, G., Avouac, J.-P., Sun, J., & Dailu, R. (2013). Spatio-temporal evolution of aseismic slip along the Haiyuan fault, China: Implications for fault frictional properties. *Earth and Planetary Science Letters*, *377*, 23–33. https://doi.org/10.1016/j.epsl.2013.07.020

Jolivet, R., Simons, M., Agram, P. S., Duputel, Z., & Shen, Z.-K. (2015). Aseismic slip and seismogenic coupling along the central San Andreas Fault. *Geophysical Research Letters*, *42*(2), 297–306. https://doi.org/10.1002/2014GL062222

Kaneko, Y., Avouac, J.-P., & Lapusta, N. (2010). Towards inferring earthquake patterns from geodetic observations of interseismic coupling. *Nature Geoscience*, *3*(5), 363–369. https://doi.org/10.1038/ngeo843

Kaneko, Y., Fialko, Y., Sandwell, D. T., Tong, X., & Furuya, M. (2013). Interseismic deformation and creep along the central section of the North Anatolian Fault (Turkey): InSAR observations and implications for rate-and-state friction properties. *Journal of Geophysical Research: Solid Earth*, *118*, 316–331. https://doi.org/10.1029/2012JB009661

Lachenbruch, A. H. (1980). Frictional heating, fluid pressure, and the resistance to fault motion. *Journal of Geophysical Research*, *85*(B11), 6097–6112. https://doi.org/10.1029/JB085iB11p06097

Lapusta, N., & Rice, J. R. (2003). Nucleation and early seismic propagation of small and large events in a crustal earthquake model. *Journal of Geophysical Research*, *108*, 2205. https://doi.org/10.1029/2001JB000793

Lapusta, N., Rice, J. R., Ben-Zion, Y., & Zheng, G. (2000). Elastodynamic analysis for slow tectonic loading with spontaneous rupture episodes on faults with rate- and state-dependent friction. *Journal of Geophysical Research*, *105*(B10), 23,765–23,789. https://doi.org/10.1029/2000JB900250

Lindsey, E. O., & Fialko, Y. (2016). Geodetic constraints on frictional properties and earthquake hazard in the Imperial Valley, Southern California. *Journal of Geophysical Research: Solid Earth*, *121*, 1097–1113. https://doi.org/10.1002/2015JB012516

Lipovsky, B. P., & Dunham, E. M. (2017). Slow-slip events on the Whillans Ice Plain, Antarctica, described using rate-and-state friction as an ice stream sliding law. *Journal of Geophysical Research: Earth Surface*, *122*, 973–1003. https://doi.org/10.1002/2016JF004183

Liu, Y., & Rice, J. R. (2005). Aseismic slip transients emerge spontaneously in three-dimensional rate and state modeling of subduction earthquake sequences. *Journal of Geophysical Research*, *110*, B08307. https://doi.org/10.1029/2004JB003424

Liu, Y., & Rice, J. R. (2007). Spontaneous and triggered aseismic deformation transients in a subduction fault model. *Journal of Geophysical Research*, *112*, B09404. https://doi.org/10.1029/2007JB004930
Marone, C. (1998). Laboratory-derived friction laws and their application to seismic faulting. *Annual Review of Earth and Planetary Sciences*, *26*(1), 643–696. https://doi.org/10.1146/annurev.earth.26.1.643
Marone, C., & Kilgore, B. (1993). Scaling of the critical slip distance for seismic faulting with shear strain in fault zones. *Nature*, *362*(6421), 618–621. https://doi.org/10.1038/362618a0
Marone, C., Raleigh, C. B., & Scholz, C. H. (1990). Frictional behavior and constitutive modeling of simulated fault gouge. *Journal of Geophysical Research*, *95*, 7007–7025. https://doi.org/10.1029/JB095iB05p07007
Mase, C. W., & Smith, L. (1987). Effects of frictional heating on the thermal, hydrologic, and mechanical response of a fault. *Journal of Geophysical Research*, *92*(B7), 6249–6272. https://doi.org/10.1029/JB092iB07p06249
Nadeau, R. M., & Johnson, L. R. (1998). Seismological studies at Parkfield VI: Moment release rates and estimates of source parameters for small repeating earthquakes. *Bulletin of the Seismological Society of America*, *88*(3), 790–814.
Nakatani, M. (2001). Conceptual and physical clarification of rate and state friction: Frictional sliding as a thermally activated rheology. *Journal of Geophysical Research*, *106*(B7), 13,347–13,380. https://doi.org/10.1029/2000JB900453
Niemeijer, A. R., & Vissers, R. L. (2014). Earthquake rupture propagation inferred from the spatial distribution of fault rock frictional properties. *Earth and Planetary Science Letters*, *396*, 154–164. https://doi.org/10.1016/j.epsl.2014.04.010
Noda, H., Nakatani, M., & Hori, T. (2013). Large nucleation before large earthquakes is sometimes skipped due to cascade-up—Implications from a rate and state simulation of faults with hierarchical asperities. *Journal of Geophysical Research: Solid Earth*, *118*(6), 2924–2952. https://doi.org/10.1002/jgrb.50211
Perfettini, H., Avouac, J.-P., Tavera, H., Kositsky, A., Nocquet, J.-M., Bondoux, F., … Soler, P. (2010). Seismic and aseismic slip on the Central Peru megathrust. *Nature*, *465*(7294), 78–81. https://doi.org/10.1038/nature09062
Persson, B. N. J. (2000). *Sliding friction: Physical principles and applications, nanoscience and technology* (2nd edn.). New York: Springer.
Rice, J. R. (1968). Mathematical analysis in the mechanics of fracture. *Fracture: An Advanced Treatise*, *2*, 191–311.
Rice, J. R. (1992). Fault stress states, pore pressure distributions, and the weakness of the San Andreas Fault. In B. Evans & T.-F. Wong (Eds.), *Fault mechanics and transport properties in rocks* (pp. 475–503). London: Academic.
Rice, J. R. (1993). Spatio-temporal complexity of slip on a fault. *Journal of Geophysical Research*, *98*(B6), 9885–9907. https://doi.org/10.1029/93JB00191
Rice, J. R., & Ruina, A. L. (1983). Stability of steady frictional slipping. *Journal of Applied Mechanics*, *50*(2), 343–349. https://doi.org/10.1115/1.3167042
Rice, J. R., Lapusta, N., & Ranjith, K. (2001). Rate and state dependent friction and the stability of sliding between elastically deformable solids. *Journal of the Mechanics and Physics of Solids*, *49*(9), 1865–1898. https://doi.org/10.1016/S0022-5096(01)00042-4
Rubin, A. M., & Ampuero, J.-P. (2005). Earthquake nucleation on (aging) rate and state faults. *Journal of Geophysical Research*, *110*, B11312. https://doi.org/10.1029/2005JB003686
Rubin, A. M., & Ampuero, J.-P. (2009). Self-similar slip pulses during rate-and-state earthquake nucleation. *Journal of Geophysical Research*, *114*, B11305. https://doi.org/10.1029/2009JB006529
Rubin, A. M., Gillard, D., & Got, J.-L. (1999). Streaks of microearthquakes along creeping faults. *Nature*, *400*(6745), 635–641. https://doi.org/10.1038/23196
Ruina, A. (1983). Slip instability and state variable friction laws. *Journal of Geophysical Research*, *88*(B12), 10,359–10,370. https://doi.org/10.1029/JB088iB12p10359
Saffer, D. M., & Tobin, H. J. (2011). Hydrogeology and mechanics of subduction zone forearcs: Fluid flow and pore pressure. *Annual Review of Earth and Planetary Sciences*, *39*(1), 157–186. https://doi.org/10.1146/annurev-earth-040610-133408
Schmitt, S. V., Segall, P., & Matsuzawa, T. (2011). Shear heating-induced thermal pressurization during earthquake nucleation. *Journal of Geophysical Research*, *116*, B06308. https://doi.org/10.1029/2010JB008035
Segall, P., & Rice, J. R. (1995). Dilatancy, compaction, and slip instability of a fluid-infiltrated fault. *Journal of Geophysical Research*, *100*, 22,155–22,171. https://doi.org/10.1029/95JB02403
Segall, P., Rubin, A. M., Bradley, A. M., & Rice, J. R. (2010). Dilatant strengthening as a mechanism for slow slip events. *Journal of Geophysical Research*, *115*, B12305. https://doi.org/10.1029/2010JB007449
Skarbek, R. M., Rempel, A. W., & Schmidt, D. A. (2012). Geologic heterogeneity can produce aseismic slip transients. *Geophysical Research Letters*, *39*, L21306. https://doi.org/10.1029/2012GL053762
Stesky, R., Brace, W., Riley, D., & Robin, P.-Y. (1974). Friction in faulted rock at high temperature and pressure. *Tectonophysics*, *23*(1), 177–203. https://doi.org/10.1016/0040-1951(74)90119-X
Stesky, R. M. (1975). Acoustic emission during high-temperature frictional sliding. *Pure and Applied Geophysics*, *113*(1), 31–43. https://doi.org/10.1007/BF01592896
Stesky, R. M. (1978). Mechanisms of high temperature frictional sliding in Westerly granite. *Canadian Journal of Earth Sciences*, *15*(3), 361–375. https://doi.org/10.1139/e78-042
Stierman, D. J. (1984). Geophysical and geological evidence for fracturing, water circulation and chemical alteration in granitic rocks adjacent to major strike-slip faults. *Journal of Geophysical Research: Solid Earth*, *89*(B7), 5849–5857. https://doi.org/10.1029/JB089iB07p05849
Tesei, T., Collettini, C., Barchi, M. R., Carpenter, B. M., & Stefano, G. D. (2014). Heterogeneous strength and fault zone complexity of carbonate-bearing thrusts with possible implications for seismicity. *Earth and Planetary Science Letters*, *408*, 307–318. https://doi.org/10.1016/j.epsl.2014.10.021
Tse, S. T., & Rice, J. R. (1986). Crustal earthquake instability in relation to the depth variation of frictional slip properties. *Journal of Geophysical Research: Solid Earth*, *91*(B9), 9452–9472. https://doi.org/10.1029/JB091iB09p09452
Tullis, T. E., & Weeks, J. D. (1986). Constitutive behavior and stability of frictional sliding of granite. *Pure and Applied Geophysics*, *124*(3), 383–414. https://doi.org/10.1007/BF00877209
Viesca, R. C. (2016a). Self-similar slip instability on interfaces with rate- and state-dependent friction. *Proceedings of the Royal Society of London A: Mathematical, Physical and Engineering Sciences*, *472*(2192). https://doi.org/10.1098/ rspa.2016.0254
Viesca, R. C. (2016b). Stable and unstable development of an interfacial sliding instability. *Physical Review E*, *93*, 060202. https://doi.org/10.1103/PhysRevE.93.060202
Villegas-lanza, J., Nocquet, J. ., Rolandone, F., Valle, M., Tavera, H., Bondoux, F., … Chlieh, M. (2016). A mixed seismic-aseismic stress release episode in the Andean subduction zone, *Nature Geoscience*, *9*(2), 150–154. https://doi.org/10.1038/ngeo2620
Waldhauser, F., Ellsworth, W. L., Schaff, D. P., & Cole, A. (2004). Streaks, multiplets, and holes: High-resolution spatio-temporal behavior of Parkfield seismicity. *Geophysical Research Letters*, *31*, L18608. https://doi.org/10.1029/2004GL020649
Williams, M. L. (1957). On the stress distribution at the base of a stationary crack. *Journal of Applied Mechanics*, *24*(1), 109–114.

Wintsch, R. P., Christoffersen, R., & Kronenberg, A. K. (1995). Fluid-rock reaction weakening of fault zones. *Journal of Geophysical Research*, *100*(B7), 13,021–13,032. https://doi.org/10.1029/94JB02622

Wojatschke, J., Scuderi, M. M., Warr, L. N., Carpenter, B. M., Saffer, D., & Marone, C. (2016). Experimental constraints on the relationship between clay abundance, clay fabric, and frictional behavior for the central deforming zone of the San Andreas Fault. *Geochemistry, Geophysics, Geosystems*, *17*(10), 3865–3881. https://doi.org/10.1002/2016GC006500